BET inhibitors reduce tumor growth in preclinical models of gastrointestinal gene signature-positive castration-resistant prostate cancer.

Shipra Shukla[1], Dan Li[1], Woo Hyun Cho[1], Dana M. Schoeps[1], Holly M. Nguyen[2], Jennifer L. Conner[2], Marjorie L. Roskes[3,4], Anisha Tehim[3,4], Gabriella Bayshtok[1], Mohini R. Pachai[1], Juan Yan[1], Nicholas A. Teri[1], Eric Campeau[5], Sarah Attwell[5], Patrick Trojer[6], Irina Ostrovnaya[7], Anuradha Gopalan[8], Ekta Khurana[3,4], Eva Corey[2], Ping Chi[1,4,9]*, and Yu Chen[1,4,9]*

[1]Human Oncology and Pathogenesis Program, Memorial Sloan Kettering Cancer Center, New York, NY, USA.
[2]Department of Urology, University of Washington, Seattle, WA, USA.
[3]Weill Cornell Medicine, New York, NY USA
[4]Weill Cornell Medical College, New York, NY, 10065, USA.
[5]Zenith Epigenetics, Calgary, AB, Canada.
[6]Triana Biomedicines, Waltham, MA.
[7]Department of Epidemiology Biostatistics, Memorial Sloan Kettering Cancer Center, New York, NY, USA.
[8]Department of Pathology and Laboratory Medicine, Memorial Sloan Kettering Cancer Center, New York, NY USA.
[9]Department of Medicine, Memorial Sloan Kettering Cancer Center, New York, NY 10065, USA.

***Correspondence:**

Yu Chen, MD, PhD
Human Oncology and Pathogenesis Program
Memorial Sloan Kettering Cancer Center
1275 York Avenue
New York, NY 10065
e-mail: cheny1@mskcc.org

Ping Chi, MD, PhD
Human Oncology and Pathogenesis Program
Memorial Sloan Kettering Cancer Center
1275 York Avenue
New York, NY 10065
e-mail: chip@mskcc.org

Conflict of Interest: E.C. was a consultant for DotQuant, and received Institutional sponsored research funding from Sanofi, Gilead, AbbVie, Genentech, Janssen Research, Astra Zeneca, GSK, Bayer Pharmaceuticals, Forma Pharmaceuticals, Foghorn, Kronos, and MarcoGenics. P.C. has received personal honoraria/advisory boards/consulting from Deciphera, Ningbo NewBay Medical Technology; P.C. has received institutional research funding from Pfizer/Array, Deciphera, Ningbo NewBay Medical Technology. Y.C. has obtained Research funding from Foghorn Therapeutics; Royalties and stock ownership from Oric Pharmaceuticals; Consultation from FogPharma and Belharra Therapeutics.

ABSTRACT

A subgroup (~20-30%) of castration-resistant prostate cancer (CRPC) aberrantly expresses a gastrointestinal (GI) transcriptome governed by two GI-lineage-restricted transcription factors, HNF1A and HNF4G. In this study, we found that expression of GI transcriptome in CRPC correlates with adverse clinical outcomes to androgen receptor signaling inhibitor treatment and shorter overall survival. Bromo- and extra-terminal domain inhibitors (BETi) downregulated HNF1A, HNF4G, and the GI transcriptome in multiple CRPC models, including cell lines, patient-derived organoids, and patient-derived xenografts, while AR and the androgen-dependent transcriptome were largely spared. Accordingly, BETi selectively inhibited growth of GI transcriptome-positive preclinical models of prostate cancer. Mechanistically, BETi inhibited BRD4 binding at enhancers globally, including both AR and HNF4G bound enhancers while gene expression was selectively perturbed. Restoration of HNF4G expression in the presence of BETi rescued target gene expression without rescuing BRD4 binding. This suggests that inhibition of master transcription factors expression underlies the selective transcriptional effects of BETi.

SIGNIFICANCE

GI transcriptome expression in CRPC is regulated by the HNF1A-HNF4G-BRD4 axis and correlates with worse clinical outcomes. Accordingly, BET inhibitors significantly reduce tumor cell growth in multiple GI-transcriptome-positive preclinical models of CRPC. Our studies point that expression of GI transcriptome could serve as a predictive biomarker to BETi therapy response.

INTRODUCTION

Lineage plasticity is increasingly being appreciated as a mechanism to evade targeted therapy by cancer cells of multiple origins and lineages. Examples include prostate cancer and EGFR-mutant lung cancer where adenocarcinomas transdifferentiate into neuroendocrine cancers under select pressure of targeted therapy. In this process, cancer cells lose dependence on the initial tumor drivers, androgen receptor (AR) in prostate cancer, and EGFR and other oncogenic RTK in lung cancer (1-3). However, in contrast to a complete switch to neuroendocrine linage, a significant fraction of prostate adenocarcinoma also exists in a heterogeneous and plastic state where cancer cells acquire features of alternate cellular lineages and states such as stem cells, basal cells, and mesenchymal cells (4-7). This poses a challenge in targeted therapy as 1) multiple dependencies exist in such tumors and 2) therapeutic targeting of the primary lineage may augment the process towards a complete lineage switch (8). Hence, combination therapies targeting more than one lineage/pathway may be more successful in such cases.

We have previously reported the activation of a gastrointestinal (GI) lineage transcriptome governed by aberrant expression of master regulators HNF1A and HNF4G in a significant fraction of castration-resistant prostate cancer (CRPC). HNF4G and HNF1A form a regulatory circuit where they influence each other's expression. Exogenous expression of either HNF4G or HNF1A is sufficient to express the GI transcriptome in LNCaP cells that do not express either transcription factor. Expression of this aberrant GI transcriptome mediates resistance to enzalutamide (9). In the present study, using two different metastatic CRPC (mCRPC) datasets, we show that increased GI transcriptome expression in patient tumors is associated with a shorter time on treatment with androgen receptor signaling inhibitors (ARSI) as well as a shorter overall survival. We hypothesized that inhibition of this transcriptome would provide therapeutic benefits in patients.

Our studies revealed that inhibitors against Bromodomain and Extraterminal (BET) family member proteins efficiently inhibit GI transcriptome expression by directly targeting *HNF1A* and *HNF4G* transcription. Finally, we show the selective growth inhibitory effect elicited by BET inhibitors either alone or in combination with enzalutamide on GI transcriptome expressing preclinical CRPC models, including patient derived organoids and xenografts.

RESULTS

Aberrant expression of GI transcriptome in CRPC correlates with adverse clinical outcomes to ARSI treatment.

The expression of GI transcriptome is governed by master regulators HNF1A and HNF4G and it is seen more prevalent in mCRPC compared to localized prostate cancer across multiple gene expression datasets (9). Experimentally, exogenous expression of HNF4G in prostate cancer cells leads to expression of the GI transcriptome and resistance to AR pathway inhibition. These data suggest a causal relationship between the expression of GI transcriptome and resistance to AR-targeted therapy (9).

Here, we sought to quantify the level of GI transcriptome expression and correlate it with clinical outcomes. We derived an *HNF signature* comprised of HNF1A, HNF4G, and their nine strong direct downstream targets and an *HNF score* derived from the summed z-scores of their gene expression. Correlation analysis performed on two clinical gene expression datasets showed that the HNF score is significantly correlated with HNF1A and HNF4G expression (**Figure S1A-B**). The HNF score also strongly correlated with the broader prostate cancer-gastrointestinal (PCa_GI) signature sum Z-score (**Figures S1A-B**). The PCa_GI signature is previously defined and derived from correlation with SPINK1 in primary prostate cancer (9). We applied HNF score to analyze two RNA-Seq datasets of CRPC tumors from patients treated with ARSIs.

The clinical trial Genetic and Molecular Mechanisms in Assessing Response in Patients with Prostate Cancer Receiving Enzalutamide Therapy (NCT02099864) prospectively enrolled 36 taxane and abiraterone naïve mCRPC patients to treatment with enzalutamide (10). Response was defined as a 50% decline in PSA after 12 weeks of treatment. Among the 25 patients with pre-treatment RNA-Seq data, we found that 20% of tumors (n=5) had a higher HNF score (Z>12) than the rest. We used this cutoff to define HNF score_High tumors **(Figure 1A).** Notably, four of five patients with HNF score_High tumors but only one of twenty patients with HNF score_Low tumors did not respond to enzalutamide treatment (Fisher's exact test P=0.012) (**Figure 1B**). Alternatively, four of seven non-responders showed a high HNF score compared to one of eighteen of responders (**Figure 1C and Figure S1C**). Global transcriptome analysis showed a significant upregulation of many GI lineage genes such as HNF1A, MUC13, UGT2B4, MIA2, and NR1H4 in enzalutamide non-responders compared to responders (**Figure S1D)**. To identify pathways enriched in non-responding tumors, we performed Gene Set Enrichment Analysis (GSEA) comparing non-responders and responders using the Molecular Signatures Database (MSigDB) comprising >20,000 gene sets and our custom gene sets. We found our previously defined PCa_GI_signature gene set as well as a gene set comprised of HNF1A targets to be significantly enriched in enzalutamide non-responders (**Figure 1C, Figure S1E, and Table S1A**). The other top significantly enriched gene sets in non-responders were related to metastasis and immune functions (**Figure S1F and Table S1A**). To understand the correlation between HNF and AR signatures, we derived an AR score as the sum z-score of AR target genes combined from two different AR signatures (11, 12). We noticed that the five tumors with high HNF scores had lower AR scores, although this correlation did not reach statistical significance (**Figure S1G**). Next, we asked if any CRPC subtypes are specifically enriched for high HNF score-expressing tumors.

Using our previously published methodology, our analysis revealed that high HNF-scored tumors showed characteristics of the AR subtype (**Figure S1H** and **Table S2)** (7).

We next analyzed the RNA-Seq data of mCRPC patients from SU2C International Dream Team and calculated the HNF score for patients for whom the overall survival and time on ARSI treatment was available (13, 14). We analyzed ARSI naïve patients going onto ARSI therapy (n=50). We ranked patients based on the tumor HNF scores annotated them into three categories: patients with a sum z-score value of >12 as in Alumkal dataset were categorized as HNF score_High while patients with a sum z-score of zero or less were categorized as HNF score_Low. The remaining patients were categorized as HNF score_Intermediate (**Figure 1D**). Kaplan Meier analysis revealed that the patients categorized as HNF score_High had the shortest median time on ARSI **(Figure 1E).** To investigate whether the poor response to ARSI would translate to shorter overall survival of these patients, we performed a Kaplan-Meier survival analysis and found that HNF score_High patients had a significantly shorter overall survival as compared to the other two cohorts (**Figure 1F**). These data suggest that increased expression of the GI transcriptome in patients is associated with worse clinical outcomes in CRPC patients. In this dataset, the HNF score in tumors correlated negatively with the AR score (**Figure S1I**). Analysis of CRPC subtype classification revealed the SCL subtype to be enriched in HNF score_High tumors while the AR-dependent subtype to be predominant in HNF score_Low tumors (**Figure S1J** and **Table S3**).

BET inhibition downregulates GI transcriptome in CRPC.

Previously, we showed that HNF4G is required for maintaining open chromatin regions and active transcription-associated epigenetic modifications such as H3K4me1 and H3K27ac at its target genes. Members of the BET family proteins, BRD2, BRD3, and BRD4 are epigenetic readers. They bind to acetylated histones through their bromodomains and facilitate the assembly of active

transcriptional complexes. In the absence of selective inhibitors against HNF1A and HNF4G, we explored the impact of targeting BET proteins on GI transcriptome expression. We used two BET inhibitors, ABBV-075 (mivebresib) and JQ1, in experiments performed on 22Rv1 cells that express the GI transcriptome. Treatment with either inhibitor for 4 hours led to a dose-dependent decrease in transcripts of *HNF1A* and *HNF4G* (**Figure 2A, B**), while the *AR* transcript was only modestly inhibited at high concentrations (**Figure S2A**). Immunoblot analysis at 24 hours post-treatment, showed reduced protein levels of HNF1A and HNF4G, as well as their downstream targets AKR1C3 and UGT2B15, while AR protein levels remained unchanged (**Figure 2C, Figure S2B**). These cells also showed a dose-dependent decrease in cell viability when treated with ABBV-075 and JQ1 (**Figure S2C**). To analyze the effect of BET inhibition on global gene expression, we performed RNA-Seq of 22Rv1 cells treated with 25 nM ABBV-075 for 24 hours. The ABBV-075 treatment led to a downregulation of the HNF signature as well as the broader PCa_GI signature **(Figure 2D)**. However, the effect of ABBV-075 on the AR transcriptome varied, as assessed using two different AR signatures with some genes such as *KLK3* that were strongly downregulated whereas *FKBP5* and *NKX3-1* were upregulated (11, 12) (**Figure 2D**). We next performed GSEA on RNA-Seq data obtained from DMSO and ABBV-075 treated cells. The topmost downregulated gene sets in ABBV-075 treated cells included the PCa_GI signature and gene sets regulated by HNF4G and HNF1A (**Figure 2E, Table S1B**).

We further analyzed three publicly available RNA-seq datasets on BET inhibitor (JQ1 and ABBV075) treatment in 22Rv1 cells (15-17). GSEA of the RNA-Seq data showed that, for both JQ1 and ABBV-075, gene sets regulated by HNF1A and HNF4G, and the PCa_GI signature, were among the most significantly downregulated gene sets. Consistent with our observations, BETi

treatment caused downregulation of *HNF1A* and *HNF4G* transcriptions but not *AR* transcript (**Figure S2D-F, Table S1C-E**).

BET inhibitors, including ZEN-3694 and NUV-868 are being evaluated in clinical trials in various cancer types, including prostate cancer (NCT02705469, NCT04471974, NCT04986423, NCT02711956, NCT05252390). We took advantage of a recently completed Phase 1b/2a clinical trial of the BET inhibitor, ZEN-3694 on a cohort of mCRPC (18). Gene expression data from pre- and post-ZEN-3694 treatment was available for four patients. Among them, pre-treatment biopsy from patient 101047 exhibited a high HNF score. RNA-Seq analysis performed on the paired biopsies of patient 101047 tumors revealed downregulation of HNF score post-ZEN-3694 treatment compared to the pretreatment biopsy. While the AR score was only modestly downregulated upon BET inhibition (**Figure 2F**). GSEA showed the downregulation of the PCa_GI_signature and HNF4G target gene sets by ZEN-3694 in the post-treatment biopsy (**Figure 2G and Figure S2G**). ZEN-3694 treatment caused downregulation of HNF1A and HNF4G but not AR in the post-treatment biopsy (**Figure S2H, Table S1F**). This anecdotal data is consistent with our data in cell lines, patient-derived organoids and PDX that BET inhibition inhibits transcription of HNF1A, HNF4G, and the GI signature.

Inhibition of HNF4G transcription principally accounts for BETi-mediated inhibition of GI transcriptome.

We asked whether the preferential inhibition of GI transcriptome over AR-regulated transcriptome by BETi treatment is due to downregulation of master transcription factors HNF4G and HNF1A but not of AR. To explore this possibility, we generated 22Rv1 derivatives that exogenously express HNF4G (HNF4G OE) or GFP (GFP OE) from the Murine Stem Cell Virus (MSCV) promoter that is not repressed with ABBV-075 (**Figure S3A-B)**. We then treated GFP OE and

HNF4G OE cells with ABBV-075 (25 nM) or DMSO for 24 hours and performed RNA-Seq analysis. We compared the effect of ABBV-075 treatment on the expression of HNF score genes between GFP or HNF4G expressing cells, using DMSO treatment as a control. We observed that restoring the expression of HNF4G can largely reverse the ABBV-075-mediated downregulation of HNF score signature genes as well as of the other HNF4G targets (**Figure 3A, Figure S3C**). Examination of individual genes shows partial (*HNF1A*) to almost complete (*CCN2*, *CLRN3*, *VIL1*) rescue of transcriptional inhibition (**Figure S3C**)). We performed HNF4G ChIP-Seq in both GFP and HNF4G overexpressing cells treated with ABBV-075 or DMSO control. ABBV-075 treatment in GFP expressing cells led to a global decrease in HNF4G binding (**Figure S3D**). In the HNF4G OE cells, HNF4G binding was maintained globally with ABBV-075 treatment consistent with restoration of HNF4G protein levels in these cells (**Figures S3B, S3D**).

Since BRD4 is the most extensively characterized member of BET family proteins, we next examined the requirement of BRD4 at the loci of these transcriptionally rescued genes. We performed BRD4 ChIP-Seq in GFP OE and HNF4G OE cells treated with ABBV-075 (25 nM for 4 hours) or DMSO. We examined BRD4 binding at BRD4 peaks that overlapped with previously defined top 1,000 HNF4G peaks (n=590), top 1,000 AR peaks (n=586), and non-overlapping BRD4 peaks (n=10,961). Exogenous expression of HNF4G led to a modest increase of BRD4 binding at HNF4G binding sites but not at AR binding sites or non-overlapping sites. ABBV-075 treatment broadly displaced BRD4 from chromatin at all BRD4 peaks and exogenous HNF4G expression did not rescue BRD4 binding (**Figure 3B**). Examination of ChIP-Seq tracks of selected genes shown in figure S3C reveals a similar level of BRD4 displacement with ABBV-075 treatment in between GFP OE and HNF4G OE cells despite their continued transcription in HNF4G OE cells (**Figure 3C**). These data suggest that BRD4 is an accessory factor rather than

the primary factor in controlling gene expression regulation. Restoration of HNF4G binding mitigates the transcriptional effects of BRD4 displacement at its target genes.

To compare the effects of HNF1A and HNF4G overexpression on BETi-mediated inhibition of target gene transcription, we overexpressed HNF1A, HNF4G, and RFP in 22Rv1 cells and performed qRT-PCR on select target genes after treatment with 25 nM ABBV-075 and 250 nM JQ1 for 24 hours. As expected, exogenous expression of HNF1A and HNF4G under the MSCV promoter led to overexpression of the respective transcripts that were insensitive to BETi. HNF4G OE led to upregulation of all transcripts tested (*HNF1A, UGT2B15, SGK2, AKR1C3, APOH, ANG, CLRN3, MUC13, and METTL7B*). Some transcripts maintained some BETi sensitivity (e.g., *HNF1A, MUC13*) and some were completely rescued (*AKR1C3, UGT2B15*). HNF1A OE upregulated *HNF4G* and most downstream genes expression. We observed almost complete transcriptional rescue of genes such as *UGT2B15, AKR1C3*, and *APOH*; a partial rescue of *HNF4G*, *SGK2*, and *CLRN3* expression and no rescue of MUC*13* and *METTL7B* expression with BETi treatments. In contrast to HNF1A, HNF4G OE showed a stronger rescue of *CLRN3*, *MUC13* and *METTL7B* transcription but a weaker rescue of *APOH* transcription suggesting target gene selectivity (**Figure S3E**).

We next performed similar studies in MSK-PCa10, an HNF high organoid model where we overexpressed HNF4G, HNF1A, and RFP and treated with ABBV-075 (25 nM) or JQ1(250 nM) or DMSO control for 24 hrs. We observed a similar and selective transcriptional rescue of HNF regulated genes by HNF1A (*UGT2B15*, *SGK2*) and HNF4G (*CLRN3*) (**Figure S3F).** These data broadly suggest that the downregulation of master transcription factors underlies the selectivity of BETi transcriptional inhibition despite the broad displacement of BET proteins from chromatin (9, 15).

GI-transcriptome-positive prostate cancer models exhibit increased sensitivity to BET inhibitors.

To examine the effect of BET inhibition on the growth of GI transcriptome-positive prostate cancer, we treated ten prostate cancer organoids derived from mCRPC patients with ABBV-075 (7, 19). Notably, we observed that organoids with a high HNF score; MSK-PCa17, MSK-PCa13, and MSK-PCa10, exhibited the lowest half-maximal inhibitory concentration (IC50) to ABBV-075 treatment, suggesting high sensitivity (**Figures 4A and S4A).** MSK-PCa17 cells had the lowest IC50 to ABBV-075 (IC50<2 nM) among all the organoids.

To identify important genes/pathways perturbed by ABBV-075, we performed RNA-Seq on MSK-PCa17 cells treated with ABBV-075 at three different concentrations (1 nM, 10 nM, and 100 nM) for four hours. Our results showed that *HNF1A* and *HNF4G* were downregulated in a dose-dependent manner, along with other signature GI transcriptome genes such as *CLRN3*, *SGK2*, and *UGT2B15* (**Figure 4B**). ABBV-075 treatment decreased the HNF score and downregulated the broader PCa_GI_signature (**Figure 4C-D**). We next performed qRT-PCR analysis in these cells with the same treatment and observed a dose-dependent decrease in expression of HNF1A, HNF4G, and downstream targets (**Figure 4E**). In MSK-PCa13 cells, the second most sensitive line, qRT-PCR analysis demonstrated a dose-dependent decrease in HNF1A, HNF4G, and downstream target genes transcript levels with ABBV-075 treatment (**Figure 4F**). MSK-PCa10, a neuroendocrine prostate cancer (NEPC) organoid with a high HNF score, showed sensitivity to BET inhibition. qRT-PCR analysis revealed no decrease in important NEPC lineage genes such as *ASCL1* and *NEUROD*. However, HNF1A and HNF4G and their downstream targets expression were suppressed by ABBV-075 in these cells (**Figure 4G**). These data suggest that organoids with a high HNF score are sensitive to growth inhibition by ABBV-075, emphasizing the potential

relevance of the GI transcriptome expression to BET inhibition response. The observed downregulation of key genes and pathways associated with the GI transcriptome supports the potential therapeutic efficacy of BET inhibition in this context. We also performed cell viability studies in organoids using JQ1 and noticed that like ABBV-075, the most sensitive models to JQ1-mediated growth inhibition expressed high HNF scores (**Figures S4B-C**).

Next, we did a preliminary screen to assess the response to BETi in vivo using a panel of twelve LuCaP patient-derived xenografts (PDXs) that are well annotated and represent the varied clinical spectrum of CRPC (20, 21). We chose pelabresib (CPI-0610) for in vivo studies because it has favorable pharmacokinetics and pharmacodynamics properties and is in late-stage clinical development (22). We treated each PDX with pelabresib or vehicle for four weeks. Fold changes in tumor volume were determined by comparing the pelabresib-treated group to the vehicle-treated group after the four-week treatment period. HNF scores for each PDX were calculated using baseline RNA-Seq data. We observed that PDXs with higher HNF scores were more sensitive to the growth-inhibitory effects of pelabresib (**Figure 5A**). We also performed immunohistochemical staining of HNF1A and HNF4G on tissue microarrays of LuCaP PDXs to validate the mRNA-based HNF score annotations. We observed that PDXs with high HNF scores showed strong nuclear staining for both HNF1A and HNF4G (**Figure 5B**). The HNF1A and HNF4G staining intensities were quantified to obtain an IHC H-score for each PDX, and the HNF score and IHC H-score showed a strong correlation (**Figure 5C**). We next examined the effect of pelabresib treatments on HNF1A and HNF4G expression in these models. A few representative examples are presented to show that pelabresib treatments effectively downregulated HNF1A and HNF4G expression (**Figure 5D-E**). These data suggest that the GI transcriptome expression in prostate cancer as assessed by HNF score, may serve as a predictive marker of prostate cancer PDXs

response to pelabresib treatment. We evaluated the growth inhibitory response of HNF4G/HNF1A+ CWR22Pc cell-derived xenograft model to pelabresib treatment in vivo. We found that pelabresib treatment inhibited the growth of the xenografts. The explanted tumors were harvested for RNA and protein extraction at two time points (2 days and end of study). qRT-PCR and immunoblotting studies showed downregulation of HNF1A, HNF4G, and their targets in pelabresib-treated tumors compared to vehicle controls (**Figure S5A-C**). Taken together, the observed correlations highlight the potential clinical relevance of the GI transcriptome in guiding BET inhibitor therapy.

To gain a comprehensive understanding of the molecular changes induced by BET inhibition, we performed single-cell RNA sequencing (scRNA-Seq) on LuCaP 70CR tumors treated with pelabresib for six days using vehicle as control. Tumors were dissociated into single-cell suspension and live cells were obtained using fluorescence-activated cell sorting. We discarded cells with mouse reads and analyzed single transcriptomes from approximately 3650 single human cells in vehicle and pelabresib-treated mice (n=2) after quality control and filtering. Dimension reduction using Uniform Manifold Approximation and Projection (UMAP) and Leiden clustering grouped tumor cells into five clusters (**Figure 6A).** In vehicle-treated mice, the majority of tumor cells grouped into cluster 1 and have characteristics of prostate adenocarcinoma including luminal markers KRT8, KRT18, FOLH1; prostate transcription factors AR, NKX3-1, FOXA1, HOXB13; and GI transcription factors HNF1A, HNF4G and downstream target like MUC13 (**Figure S6A**). In addition, a fraction of cells grouped into cluster 4, which maintained prostate lineage markers and is additionally characterized by expression of proliferation genes, suggesting this is the proliferative cluster (**Figures 6B and S6A-B**). Treatment with pelabresib resulted in a decrease in clusters 1 and 4 cell population and an increase/emergence of clusters 2, 3, and 5

(**Figure 6A**). These three clusters all expressed senescence-related genes and exhibited a high senescence score, with the small cluster 5 exhibiting high scores for both proliferation and senescence (**Figures 6C and S6B**). We performed Ki67 and p21 immunohistochemical staining on pelabresib treated tumors as markers of proliferation and senescence, respectively. We noticed a decrease in Ki67 staining and an increase in p21 staining in pelabresib treated tumors compared to vehicle treated controls (**Figure 6D**). These data suggest that pelabresib treatment inhibits proliferation and induces senescence in these preclinical models.

Pelabresib treatment led to robust decrease in *HNF1A* and modest decrease in *HNF4G* expression assess by scRNA-seq transcript levels and by IHC (**Figure 6E-G**), consistent with in vitro data (**Figures 2A-B, 4B, 4F**). To quantify the downstream GI transcriptome, we assigned the previously defined HNF and AR scores to each single cell in both treatment conditions. Pelabresib treatment led to a significant decrease in the HNF score, suggesting an effect on the GI transcriptome (**Figures 6H and S6C**). In contrast, AR expression was not suppressed, and AR score did not decrease with pelabresib treatment (**Figures 6I-J**). This is consistent with bulk RNA-Seq data on 22Rv1 cells (**Figures 2D and S2A**). We next performed pseudobulk analysis pooling all single-cell transcriptomic data of each condition to identify differentially expressed genes between pelabresib and vehicle treatment. GSEA analysis of the pseudobulk data showed enrichment of PCa_GI, HNF1A, and HNF4G targets, as well as cell cycle-related gene sets in pelabresib downregulated genes. Senescence-related gene sets were enriched in pelabresib upregulated genes **(Figure S6D).** Collectively, these data indicate that BETi inhibits the GI transcriptome, inhibits proliferation, and induces senescence in GI transcriptome-positive prostate cancer.

Combination efficacy of enzalutamide and pelabresib in AR-positive CRPC PDX models.

Next, we asked whether BET inhibition could further synergize with AR inhibition in CRPC by targeting a parallel survival pathway of the GI transcriptome. For this we used CRPC PDXs with varied levels of HNF scores; LuCaP 70CR (AR^{pos} HNF^{high}), LuCaP 77CR (AR^{pos} HNF^{high}), LuCaP 35CR (AR^{pos} HNF^{low}), LuCaP 145.2 (NEPC, HNF^{neg}), LuCaP 49 (NEPC, HNF^{neg}) and LuCaP 93 (NEPC, HNF^{neg}) and treated them with enzalutamide, pelabresib and a combination of enzalutamide and pelabresib. In LuCaP 70CR, a castration resistant PDX model, enzalutamide treatment reduced tumor growth rate. Pelabresib treatment induced stronger growth inhibition and the combination of pelabresib with enzalutamide had the most potent growth inhibitory effects (**Figure 7A**). Immunoblot analysis performed on tumors collected at the end of the experiment showed a decrease in the protein level of HNF1A in tumors treated with pelabresib alone or in combination with enzalutamide. No significant change in AR protein level was detected with any of the drug treatments **(Figure 7B).** qRT-PCR analysis performed using RNA extracted from the end-of-study tumors revealed a decrease in selected GI lineage gene transcripts such as HNF1A and MUC13. Enzalutamide treatment decreased AR-target genes expression, and the combination treatment decreased both AR and HNF1A/HNF4G-target genes expression (**Figure 7C**).

LuCaP 35CR is a castration resistant PDX model with a low HNF score. LuCaP 35CR tumors were treated with vehicle, enzalutamide, pelabresib, and the combination of pelabresib with enzalutamide for four weeks. Tumors showed resistance to enzalutamide treatment. Pelabresib as a single agent, had moderate response. However, the combination treatment of pelabresib and enzalutamide significantly reduced tumor growth **(Figure 7D).** Immunoblot analysis on protein lysates from end-of-study tumors revealed that enzalutamide treatment led to an increase in protein

levels of HNF4G, HNF1A, and MUC13 (**Figure 7E).** The increase in HNF1A and HNF4G protein after enzalutamide treatment was also observed by IHC of tumor samples (**Figure S7A**). Previously, we have noted similar observations in LNCaP/AR tumors treated with enzalutamide (9). Importantly, the increase in GI gene expression induced by enzalutamide treatment could be effectively inhibited by combining pelabresib with enzalutamide (**Figure 7E**). RNA-Seq analysis was performed on LuCaP 35CR tumors to study global transcriptome changes under different treatment conditions. Enzalutamide treatment significantly increased the HNF score. Pelabresib decreased HNF1A expression and the HNF score, and in combination with enzalutamide, reversed the enzalutamide-induced increase in the HNF score (**Figures 7F and S7B**). The AR score decreased with enzalutamide alone and with enzalutamide and pelabresib combination treatment but not with pelabresib treatment alone (**Figures 7F and S7B**).

Similar observations were noted when we performed a short-term treatment study using LuCaP 77CR, a castration resistant, a high HNF score, and an AR-positive model. Enzalutamide alone did not cause any significant growth inhibition. In contrast, pelabresib treatment either alone or in combination with enzalutamide significantly reduced the growth of LuCaP 77CR **(Figure 7G).** Immunoblot analysis of protein lysates prepared from end-of-study tumors revealed that pelabresib treatment either alone or in combination with enzalutamide led to a decrease in protein levels of HNF4G and HNF1A. AR protein level remained unchanged under all treatment conditions (**Figure 7H**). The effect of pelabresib on HNF1A and HNF4G protein levels was also confirmed by IHC (**Figure S7C**). RNA-Seq analysis performed on end-of-study tumors revealed a decrease in *HNF1A* expression as well as the HNF score with both the pelabresib and the combination treatment, while neither *AR* expression nor the AR score altered with any of the treatments **(Figures 7I and S7D).**

Taken together, across different GI transcriptome-expressing CRPC PDX models, consistent pelabresib-mediated growth inhibition was observed. Importantly, global transcriptome analysis consistently showed robust downregulation of HNF1A, HNF4G and the HNF score with pelabresib treatment in all the PDX models assayed. Furthermore, tumor growth of the GI transcriptome expression negative PDX models (LuCaP 49, LuCaP 145.2 and LuCaP 93) was not inhibited by pelabresib treatment **(Figure 7J).** Taken together, these data suggest a selective growth inhibitory effect of BET inhibitors on GI transcriptome-expressing models.

DISCUSSION

In prostate cancer, lineage plasticity results in extensive reprogramming of the epigenetic landscape, including changes in the cistrome of the master transcription factors FOXA1 (23) or switch to other master transcription factors, such as loss of AR and gain of ASCL1 or NEUROD1 in neuroendocrine prostate cancer (24, 25). We have uncovered that aberrant upregulation of gastrointestinal master regulators HNF4G and HNF1A alters enhancer landscape and chromatin accessibility conducive to the expression of GI-specific transcriptome in prostate cancer cells. In the present study, we found that a high GI transcriptome expression in mCRPC tumors is predictive of poor response to AR-targeted therapies and a shorter overall patients' survival. Our previous studies have shown that genetic depletion of either HNF1A or HNF4G inhibits GI transcriptome expression. Thus, we reasoned that pharmacological targeting of either HNF1A or HNF4G would be sufficient for therapeutic studies. HNF4G is an orphan nuclear receptor with no well-characterized ligand and HNF1A is a homeobox domain containing transcription factor lacking any small molecule binding pocket. Due to expected roadblocks in identifying small molecule

inhibitors regulating the activity of these transcription factors, we focused on an alternative approach of inhibiting HNF1A and HNF4G transcription.

Epigenetic therapy has been proposed to target specific lineage states in prostate cancer. Prior studies have suggested that BET, P300/CBP, LSD1, EZH2, and SWI/SNF inhibitors can disrupt AR-mediated transcriptional activity (16, 17, 26-29). Several studies have shown BRD4 as an important cofactor required for AR transcriptional activity (16, 26). One important caveat of these studies is that cells were hormone starved in charcoal-stripped media and the addition of DHT together with BETi led to severely impaired AR target gene expression compared to the addition of DHT alone. In these studies, and consistent with our observations, the transcription of AR itself was unaffected by BET inhibition. In our studies using 22Rv1 cells, a panel of patient-derived organoids and a panel of LuCaP PDX models, BRD4 inhibition did not consistently inhibit the AR-regulated transcriptome, though it did inhibit it in LuCaP 77CR.

Despite early excitement of BET inhibitors, the clinical data have shown only modest activity. One limitation has been on target toxicity and early trials of BET inhibitors have shown dose-limiting GI and thrombocytopenia toxicities. Encouragingly, recently a trial of ZEN-3694 was well tolerated at doses where BET targets showed a four-fold mean decrease in expression with no dose-limiting toxicities. ZEN-3694 showed prolonged disease stabilization in a subset of patients who exhibited ARSI refractory disease. Although the trial could not precisely define any biomarkers predictive of ZEN-3694 response, patients with low baseline AR signaling in tumors demonstrated longer rPFS than patients with high AR signaling (median rPFS 10.4 vs. 4.3 months). This data indicates that tumors with a high HNF score expression show more stem-cell-like features and low AR activity and may benefit by BETi. There were four patients with pre-and post-treatment biopsy and RNA-seq. In the one patient with an elevated HNF4 signature, treatment with

ZEN-3694 significantly inhibited the signature. In terms of AR signaling, approximately, ~30% of patients experienced an acute rise of PSA upon starting the drug and this rise was associated with longer progression-free survival, a feature that distinguishes BETi from ARSIs (18). A serum PSA decline of 50% or more (PSA50) with ZEN-3694 treatment was seen in only 10% of patients and was not correlated with response to treatment. In another clinical trial using a different BETi GS-5829, only one out of thirty-one patients showed a PSA50 decline (30). These data are consistent with our results and indicate that AR transcriptome is not inhibited by BETi in patients and AR-independent mechanisms may contribute to BET inhibitor response (18).

These data suggest the need for a biomarker-based BETi therapeutic strategy in combination with ARSIs. As a future direction, we are evaluating immunohistochemical staining of HNF4G or HNF1A on pre-treatment biopsies as a biomarker of elevated GI signaling in CRPCs. In PDXs, we found an excellent correlation between HNF4G and HNF1A IHC. Our previously published study showed that GI subtype characterized by HNF4G IHC is correlated with GI-transcriptome expression in CRPCs (9). Taken together, our findings not only implicate the poor prognosis of GI transcriptome expressing prostate cancer but also emphasize this subset to be vulnerable to BET inhibitors-mediated growth inhibition. Therefore, our studies have important clinical implications, and we propose that a high HNF1A/HNF4G transcriptional activity in CRPC tumors is a biomarker of an aggressive, ARSI-resistant disease that can be managed by treatment with BET inhibitors.

METHODS

Sex as a biological variable

Our study exclusively examined male mice because the disease modeled is only relevant in males.

Statistics

All statistical analyses were performed using GraphPad Prism 10 (GraphPad Software). Unless otherwise noted in the figure legends, all data are shown as the mean ± SEM combined with a 2-tailed, unpaired *t* test for statistical comparisons between 2 groups, and a log-rank (Mantel-Cox) test for survival analyses. A *P* value of less than 0.05 was considered statistically significant. All experiments shown were repeated at least twice.

Study Approvals

The LuCaP patient-derived xenografts were acquired from rapid autopsies under University of Washington IRB 2341. The MSK-PCa patient-derived organoids were acquired from biopsies under Memorial Sloan Kettering IRB 12-245 or 06-107. All PDX experiments performed at University of Washington were approved under IACUC 3202-01 and all PDX experiments performed at Memorial Sloan Kettering were approved under IACUC 11-12-027.

Mouse procedures

CB17 SCID male mice (Charles River) were castrated and, 2 weeks after castration, were subcutaneously implanted with tumor bits of LuCaP 35CR, 70CR, 77CR. LuCaP 49, 93 and 145.2 were implanted in intact CB17 SCID male mice. When tumors exceeded 100 mm^3, animals were randomized to control and treatment groups (n = 3–6 per group). Treatment with enzalutamide (50 mg/kg, once a day), pelabresib (30 mg/Kg, twice daily), enzalutamide and pelabresib combination or vehicle was begun at a tumor size of 100 mm^3. Mice were treated until the end of the experiments. Tumor volumes were monitored twice weekly. The research personnel measuring tumors were blinded to the treatment group assignment of mice.

For CWR22PC xenograft studies, 2.0×10^6 cells resuspended in 100 µL of 1:1 mix of growth media and Matrigel (BD Biosciences) were subcutaneously injected into 6-8 weeks old CB17-

SCID male mice (Taconic). Tumor sizes were measured weekly with calipers starting 4 weeks after xenografting and were calculated using the following formula: tumor volume = (D2 × d2× h2)/6, whereby D, d and h refers to long diameter, short diameter, and height of the tumor, respectively. Treatment with pelabresib (30mg/kg) or vehicle was begun at a tumor size of 100 mm^3. Mice were treated twice daily until the end of the experiments. Two mice from each group were collected post two days start of treatment.

Gene expression analysis

RNA-seq was performed by the MSKCC Integrated Genomics Operation (IGO) core facility using poly-A capture. The libraries were sequenced on an Illumina NovaSeq 6000 platform with 100 bp paired-end reads to obtain a minimum yield of 40 million reads per sample. The sequence data were processed and mapped to the human reference genome (hg38) or mouse reference genome (mm10) using STAR (RRID:SCR_004463), version 2.3 (31). Gene expression was quantified as transcripts per million (TPM) using "edge" R package (32) and log2 transformed. GSEA was performed using JAVA GSEA 2.0 program, using a difference of mean between replicates and gene permutation (33). The gene sets used were the Broad Molecular Signatures Database gene sets v7, c2 (curated gene sets), c5 (gene ontology gene sets), c6 (oncogenic signatures), c7 (immunologic signatures) as well as custom gene sets generated by us.

Single Cell RNA-seq

Subcutaneous PDX tumors were harvested after vehicle or pelabresib treatment (n=2 mice for each condition). The tumors were dissociated into single-cell suspension using the tumor dissociation kit (Miltenyi Biotec, 130-095-929) following the manufacturer's protocol. Live DAPI-negative, single tumor cells were sorted out by flow cytometry. For each sample, 5,000 cells were directly processed with 10X genomics Chromium Single Cell 3' GEM, Library & Gel Bead Kit v3

according to the manufacturer's specifications. For each sample, 200 million reads were acquired on NovaSeq platform S4 flow cell. See extended methods for data analysis.

Immunohistochemistry

The IHC were performed on an automated Ventana Discovery Ultra Automated IHC Platform. Briefly, Formalin-fixed paraffin-embedded (FFPE) tissue sections were de-paraffinized and endogenous peroxidase was inactivated. Antigen retrieval was performed by warming up slides to 100 °C and incubating for 4 Minutes (Cell Conditioner #1). Sections were then incubated sequentially with the primary antibody overnight, post-primary for 15 minutes and polymer for 25 minutes, followed by a 10-minute colorimetric development with diaminobenzidine (DAB).

Analysis of HNF1A and HNF4G IHC in LuCaP tissue microarrays (TMA)

IHC was performed in triplicates on tissue microarrays composed of forty different PDX cores each mounted in triplicates. Staining intensities were quantified using Q-Path software (https://qupath.github.io). Multiple areas were randomly selected in all three replicates of each PDX core. Percentage and intensity of nuclear DAB staining were then measured within these regions of interests to obtain a mean H-score. The H-score was calculated as follows: H-score = (1x no of cells with weak nuclear staining) + (2x no of cells with moderate nuclear staining) + (3x no of cells with strong nuclear staining). HNF4G and HNF1A staining were similarly quantified in Figure 5 and Figure 6 (n=2). For Ki67 and p21 staining, instead of H-scores, total number of positively stained cells were determined by selecting different areas of images to include a total of 5000 cells per treatment condition (n=2).

Chromatin Immunoprecipitation and Sequencing

Chromatin isolation from cell lines and immunoprecipitation was performed following the protocol previously described (9). See extended methods for details.

HNF signature and HNF score

HNF signature consists of *HNF1A*, *HNF4G*, and their nine strong direct downstream targets (*AKR1C3*, *ANG*, *APOH*, *CLRN3*, *GAS2*, *METTL7B*, *MUC13*, *SGK2*, and *UGT2B15*). The nine candidate genes were chosen if their expression changed with HNF1A/HNF4G knockdown or overexpression in 22Rv1 and LNCaP cells respectively and whether their loci showed a direct HNF1A and HNF4G binding (GSE85559 and unpublished data). An HNF score is derived from the summed z-scores of HNF signature genes expression.

AR score

Two previously defined AR signatures (10-gene AR signature and Hieronymus AR Signature) were combined to generate a broader AR signature (11, 12). The AR score is the summed z-scores of AR signature genes expression.

Data availability

Gene Expression Omnibus (GEO) (RRID:SCR_005012) Accession Numbers of Datasets Generated:

- GSE253805: RNA-Seq expression profile of CRPC PDX LuCaP 77CR with BET inhibitor pelabresib and AR inhibitor enzalutamide treatment.
- GSE253806.: scRNA-Seq expression profile of CRPC PDX LuCaP 70CR with BET inhibitor pelabresib treatment.
- GSE254665: RNA-Seq expression profile of CRPC PDX LuCaP 35CR when treated with BET inhibitor pelabresib and AR inhibitor enzalutamide.
- GSE254733: RNA-Seq expression profile of 22Rv1 cells with GFP or HNF4G exogenous expression when treated with BET inhibitor ABBV-075.

- GSE254869: BRD4 ChIP-Seq in 22Rv1 cells exogenously expressing HNF4G or GFP and treated with BET inhibitor ABBV-075.
- GSE254870: BET inhibitor ABBV-075 perturbed pathways in prostate cancer organoid MSK-PCa17.

The data values of all graphs and values behind any reported means in the manuscript are provided in a spreadsheet labeled Supporting data values.

AUTHOR CONTRIBUTION

Experimental design: S.S., P.C., and Y.C.; Western blots and qRT-PCRs: S.S., D.M.S. and J.Y.; IHC: W.H.C, ChIP-Seq, RNA-Seq, Single cell-RNA-Seq: S.S; Analysis of ChIP-Seq, RNA-Seq, and scRNA-Seq: D.L.; Cell viability assays: S.S.; Bioinformatic/Biostatistics Analysis: S.S., D.L., I.O., M.R., T.A, E.K. and Y.C. Mouse experiments design and execution: E.C., H.N., J.C., G.B., D.M.S., N.T., M.P; Resources sharing: E.C., A.G., E.C., S.A., and P.T.; Pathology supervision: A.G.; Manuscript writing: S.S., and Y.C. All authors reviewed and edited the manuscript.

ACKNOWLEDGEMENT

Pelabresib was generously provided for in vivo experiments by Constellation Pharmaceuticals. Establishment of LuCaP PDXs was supported by the Pacific Northwest Prostate Cancer SPORE (P50CA97186), the P01 NIH grant (P01CA163227), and the Institute for Prostate Cancer Research. We would like to thank the patients who generously donated tissue that made this research possible. We would also like to thank Comparative Medicine Animal Caregivers for their assistance with the LuCaP PDX work. We acknowledge the use of the Integrated Genomics Operation Core. This work was funded by the NCI Cancer Center Grant (P30CA008748), the NCI SPORE (P50CA221745 to Y.C., P.C., A.G.), the Cancer Moonshot Drug Resistance and

Sensitivity Network (DRSN) (U54CA224079 to Y.C.), R01CA193837, R01CA208100, the Prostate Cancer Foundation (Y.C.), the STARR Cancer Consortium (Y.C. and P.C.)., and the Geoffrey Beene Cancer Center (Y.C. and P.C.).

REFERENCES:

1. Sequist LV, Waltman BA, Dias-Santagata D, Digumarthy S, Turke AB, Fidias P, et al. Genotypic and histological evolution of lung cancers acquiring resistance to EGFR inhibitors. *Sci Transl Med.* 2011;3(75):75ra26.
2. Beltran H, Prandi D, Mosquera JM, Benelli M, Puca L, Cyrta J, et al. Divergent clonal evolution of castration resistant neuroendocrine prostate cancer. *Nat Med.* 2016;22(3):298-305.
3. Quintanal-Villalonga Á, Chan JM, Yu HA, Pe'er D, Sawyers CL, Sen T, and Rudin CM. Lineage plasticity in cancer: a shared pathway of therapeutic resistance. *Nat Rev Clin Oncol.* 2020;17(6):360–71.
4. Watson PA, Arora VK, and Sawyers CL. Emerging mechanisms of resistance to androgen receptor inhibitors in prostate cancer. *Nat Rev Cancer.* 2015;15(12):701-11.
5. Labrecque MP, Coleman IM, Brown LG, True LD, Kollath L, Lakely B, et al. Molecular profiling stratifies diverse phenotypes of treatment-refractory metastatic castration-resistant prostate cancer. *J Clin Invest.* 2019;129(10):4492-505.
6. Han H, Wang Y, Curto J, Gurrapu S, Laudato S, Rumandla A, et al. Mesenchymal and stem-like prostate cancer linked to therapy-induced lineage plasticity and metastasis. *Cell Rep.* 2022;39(1):110595.
7. Tang F, Xu D, Wang S, Wong CK, Martinez-Fundichely A, Lee CJ, et al. Chromatin profiles classify castration-resistant prostate cancers suggesting therapeutic targets. *Science.* 2022;376(6596):eabe1505.
8. Mu P, Zhang Z, Benelli M, Karthaus WR, Hoover E, Chen CC, et al. SOX2 promotes lineage plasticity and antiandrogen resistance in TP53- and RB1-deficient prostate cancer. *Science.* 2017;355(6320):84-8.
9. Shukla S, Cyrta J, Murphy DA, Walczak EG, Ran L, Agrawal P, et al. Aberrant Activation of a Gastrointestinal Transcriptional Circuit in Prostate Cancer Mediates Castration Resistance. *Cancer Cell.* 2017;32(6):792-806.e7.
10. Alumkal JJ, Sun D, Lu E, Beer TM, Thomas GV, Latour E, et al. Transcriptional profiling identifies an androgen receptor activity-low, stemness program associated with enzalutamide resistance. *Proc Natl Acad Sci U S A.* 2020;117(22):12315-23.
11. Bluemn EG, Coleman IM, Lucas JM, Coleman RT, Hernandez-Lopez S, Tharakan R, et al. Androgen Receptor Pathway-Independent Prostate Cancer Is Sustained through FGF Signaling. *Cancer Cell.* 2017;32(4):474-89 e6.
12. Hieronymus H, Lamb J, Ross KN, Peng XP, Clement C, Rodina A, et al. Gene expression signature-based chemical genomic prediction identifies a novel class of HSP90 pathway modulators. *Cancer Cell.* 2006;10(4):321-30.
13. Robinson D, Van Allen EM, Wu YM, Schultz N, Lonigro RJ, Mosquera JM, et al. Integrative clinical genomics of advanced prostate cancer. *Cell.* 2015;161(5):1215-28.
14. Abida W, Cyrta J, Heller G, Prandi D, Armenia J, Coleman I, et al. Genomic correlates of clinical outcome in advanced prostate cancer. *Proc Natl Acad Sci U S A.* 2019;116(23):11428-36.
15. Cai L, Tsai YH, Wang P, Wang J, Li D, Fan H, et al. ZFX Mediates Non-canonical Oncogenic Functions of the Androgen Receptor Splice Variant 7 in Castrate-Resistant Prostate Cancer. *Mol Cell.* 2018;72(2):341-54 e6.
16. Faivre EJ, McDaniel KF, Albert DH, Mantena SR, Plotnik JP, Wilcox D, et al. Selective inhibition of the BD2 bromodomain of BET proteins in prostate cancer. *Nature.* 2020;578(7794):306-10.
17. Welti J, Sharp A, Brooks N, Yuan W, McNair C, Chand SN, et al. Targeting the p300/CBP Axis in Lethal Prostate Cancer. *Cancer Discov.* 2021;11(5):1118-37.

18. Aggarwal RR, Schweizer MT, Nanus DM, Pantuck AJ, Heath EI, Campeau E, et al. A Phase Ib/IIa Study of the Pan-BET Inhibitor ZEN-3694 in Combination with Enzalutamide in Patients with Metastatic Castration-resistant Prostate Cancer. *Clin Cancer Res.* 2020;26(20):5338-47.
19. Gao D, Vela I, Sboner A, Iaquinta PJ, Karthaus WR, Gopalan A, et al. Organoid cultures derived from patients with advanced prostate cancer. *Cell.* 2014;159(1):176-87.
20. Lam HM, McMullin R, Nguyen HM, Coleman I, Gormley M, Gulati R, et al. Characterization of an Abiraterone Ultraresponsive Phenotype in Castration-Resistant Prostate Cancer Patient-Derived Xenografts. *Clin Cancer Res.* 2017;23(9):2301-12.
21. Nguyen HM, Vessella RL, Morrissey C, Brown LG, Coleman IM, Higano CS, et al. LuCaP Prostate Cancer Patient-Derived Xenografts Reflect the Molecular Heterogeneity of Advanced Disease an--d Serve as Models for Evaluating Cancer Therapeutics. *Prostate.* 2017;77(6):654-71.
22. Albrecht BK, Gehling VS, Hewitt MC, Vaswani RG, Cote A, Leblanc Y, et al. Identification of a Benzoisoxazoloazepine Inhibitor (CPI-0610) of the Bromodomain and Extra-Terminal (BET) Family as a Candidate for Human Clinical Trials. *J Med Chem.* 2016;59(4):1330-9.
23. Baca SC, Takeda DY, Seo JH, Hwang J, Ku SY, Arafeh R, et al. Reprogramming of the FOXA1 cistrome in treatment-emergent neuroendocrine prostate cancer. *Nat Commun.* 2021;12(1):1979.
24. Cejas P, Xie Y, Font-Tello A, Lim K, Syamala S, Qiu X, et al. Subtype heterogeneity and epigenetic convergence in neuroendocrine prostate cancer. *Nat Commun.* 2021;12(1):5775.
25. Chen CC, Tran W, Song K, Sugimoto T, Obusan MB, Wang L, et al. Temporal evolution reveals bifurcated lineages in aggressive neuroendocrine small cell prostate cancer trans-differentiation. *Cancer Cell.* 2023;41(12):2066-82 e9.
26. Asangani IA, Dommeti VL, Wang X, Malik R, Cieslik M, Yang R, et al. Therapeutic targeting of BET bromodomain proteins in castration-resistant prostate cancer. *Nature.* 2014;510(7504):278-82.
27. Lasko LM, Jakob CG, Edalji RP, Qiu W, Montgomery D, Digiammarino EL, et al. Discovery of a selective catalytic p300/CBP inhibitor that targets lineage-specific tumours. *Nature.* 2017;550(7674):128-32.
28. Xiao L, Parolia A, Qiao Y, Bawa P, Eyunni S, Mannan R, et al. Targeting SWI/SNF ATPases in enhancer-addicted prostate cancer. *Nature.* 2022;601(7893):434-9.
29. Li M, Liu M, Han W, Wang Z, Han D, Patalano S, et al. LSD1 Inhibition Disrupts Super-Enhancer-Driven Oncogenic Transcriptional Programs in Castration-Resistant Prostate Cancer. *Cancer Res.* 2023;83(10):1684-98.
30. Aggarwal R, Starodub AN, Koh BD, Xing G, Armstrong AJ, and Carducci MA. Phase Ib Study of the BET Inhibitor GS-5829 as Monotherapy and Combined with Enzalutamide in Patients with Metastatic Castration-Resistant Prostate Cancer. *Clin Cancer Res.* 2022;28(18):3979-89.
31. Dobin A, Davis CA, Schlesinger F, Drenkow J, Zaleski C, Jha S, et al. STAR: ultrafast universal RNA-seq aligner. *Bioinformatics.* 2013;29(1):15-21.
32. Robinson MD, McCarthy DJ, and Smyth GK. edgeR: a Bioconductor package for differential expression analysis of digital gene expression data. *Bioinformatics.* 2010;26(1):139-40.
33. Subramanian A, Tamayo P, Mootha VK, Mukherjee S, Ebert BL, Gillette MA, et al. Gene set enrichment analysis: a knowledge-based approach for interpreting genome-wide expression profiles. *Proc Natl Acad Sci U S A.* 2005;102(43):15545-50.

FIGURE LEGENDS

Figure 1. A high HNF score in CRPC correlates with adverse clinical outcomes.

(**A**) Patient stratification based on HNF scores in the Alumkal dataset. Each dot represents one patient. HNF score was calculated as the log2 sum z-score of mRNA expression of eleven genes. A sum z-score of >=12 was annotated as a high HNF score and <12 as a low HNF score. See methods for details.

(**B**) Enzalutamide response of patient tumors with high and low HNF scores. Statistical significance is determined using Fisher's exact test.

(**C**) Comparison of HNF scores between enzalutamide non-responders and responders (top) and GSEA plot of PCa_GI Gene signature (bottom) in enzalutamide non-responders compared to responders. *P* by unpaired, 2-tailed t-test. NES: Normalized enrichment score. FDR: False discovery rate.

(**D**) Patient stratification based on HNF score expression in SU2C dataset. Each dot represents one patient. Tumors with a sum z-score of >=12 were annotated as expressing high HNF score; <=0 as low HNF score and a value between 0-12 as intermediate HNF_score. See methods for details.

(**E**) Kaplan–Meier curve comparing ARSI outcome measures between the three groups stratified by HNF scores. *P* by log-rank (Mantel-Cox) test.

(**F**) Kaplan–Meier curve comparing overall survival outcome between the three groups stratified by HNF scores. *P* by log-rank (Mantel-Cox) test.

Figure 2. BET inhibitors downregulate the expression of *HNF4G* and *HNF1A* and their transcriptional signature.

(**A**) qRT-PCR showing expression of HNF1A after 4 hours of treatment with ABBV-075 and JQ1 at indicated doses.

(**B**) qRT-PCR showing expression of HNF4G after 4 hours of treatment with ABBV-075 and JQ1 at indicated doses.

(**C**) A representative immunoblot of 22Rv1 cells treated with JQ (0.5 μM), ABBV-075 (50 nM), and DMSO control for 24 hours against the indicated proteins (top) and (bottom) bar graph showing fold change in β-actin normalized band intensities of JQ1 and ABBV-075 treated samples over DMSO controls (n=2).

(**D**) Heatmap of RNA-Seq expression of HNF signature genes in 22Rv1 cells after treatment with 25 nM ABBV-075 for 24 hours (top). The two bottom heatmaps show the modulation of AR target genes with ABBV-075 treatment using two different AR gene signatures. Data is plotted as the log2 difference in gene expression between ABBV-075 and DMSO treated cells. Unadjusted P-values are shown: *P < 0.05, **P < 0.01, ***P < 0.001, and ****P < 0.0001.

(**E**) Global representation of GSEA analysis of RNA-Seq gene expression data set of 22RV1 cells treated with 25 nM ABBV-075 for 24 hours. X-axis shows the normalized enrichment score, and y-axis is the FDR q-value. The PCa_GI and the HNF1A, and HNF4G-regulated gene sets are indicated in red. GSEA plot of PCa_GI gene signature is shown in the middle. A bar diagram on the right shows the expression of AR, HNF1A, and HNF4G. NES: Normalized enrichment score. FDR: False discovery rate.

(**F**) Modulation of HNF and AR scores by BETi ZEN-3694 in paired tumor biopsies of patient 101047.

(**G**) GSEA plots of PCa_GI Gene signature in ZEN-3694 treated tumors compared to pretreated tumor. NES: Normalized enrichment score. FDR: False discovery rate.

Figure 3. Inhibition of HNF4G transcription accounts for BETi mediated inhibition of GI transcriptome.

(**A**) Violin plot of log2 fold changes in expression of HNF score genes by ABBV-075 treatment in 22Rv1 cells exogenously expressing GFP or HNF4G compared with DMSO control. The

median is represented by a solid line, while the first and third quartiles are indicated by dashed lines with all dots plotted. Statistical analysis was performed using a 2-tailed paired t-test.

(**B**) Histograms (top) show the average normalized tag counts of AR and HNF4G in parental 22Rv1 cells and that of BRD4 in GFP or HNF4G expressing 22Rv1 cells treated with ABBV-075 or DMSO at top 1,000 HNF4G, 1,000 AR binding sites and BRD4 only enhancer binding sites. Heatmap shows the tag densities of HNF4G, AR, and that of BRD4 at HNF4G (top) or AR (middle) binding sites. Bottom panel show the tag densities of BRD4 at 10,961 BRD4 only sites in GFP or HNF4G expressing 22Rv1 cells treated with ABBV-075 or DMSO.

(**C**) ChIP-seq profiles of HNF4G in parental 22Rv1 cells and BRD4 (DMSO treatment), and BRD4 (ABBV-075 treatment) in GFP or HNF4G expressing 22Rv1 cells at selected HNF4G target genes loci; *HNF1A*, *CCN2*, *CLRN3*, *F5*, *MUC13*, and *VIL1* in top to bottom order.

Figure 4. Patient-derived organoids with high HNF scores show increased sensitivity to BETi-mediated growth inhibition.

(**A**) IC50 of ABBV-075 in a panel of patient-derived tumor biopsies grown as organoids. The left Y-axis plots the HNF scores of each organoid and the right Y-axis shows the IC50 values.

(**B**) RNA-Seq gene expression changes of selected genes at different doses of ABBV-075 treatment of MSK-PCa17 cells compared to DMSO control. Data is presented as log2 fold difference in expression (ABBV-075 vs DMSO).

(**C**) A bar graph showing changes in HNF score expression in MSK-PCa17 cells at different doses of ABBV-075 treatment compared to DMSO control.

(**D**) GSEA analysis indicating the negative enrichment of PCa_GI gene signature gene set in MSK-PCa17 cells treated with ABBV-075 (10 nM) compared to DMSO control. NES: Normalized enrichment score.

(**E**) qRT-PCR showing expression of selected genes after 4 hours of treatment with ABBV-075 at indicated doses in MSK-PCa17 cells (n=3).

(**F**) qRT-PCR showing expression of selected genes after 4 hours of treatment with ABBV-075 at indicated doses in MSK-PCa13 cells (n=3).

(**G**) qRT-PCR showing expression of selected genes after 4 hours of treatment with ABBV-075 at indicated doses in MSK-PCa10 cells (n=3).

Unpaired, 2-tailed t-test. *P < 0.05, **P < 0.01, ***P < 0.001, and ****P < 0.0001.

Figure 5. CRPC PDXs expressing high HNF score are sensitive to BET inhibition.

(**A**) Treatment response of LuCaP PDXs when treated with pelabresib (30 mg/kg) or vehicle (1% carboxymethyl cellulose) twice a day. Treatment was started when tumors reached a volume of approximately 100 mm^3. Data is plotted as the fold change in tumor volume between pelabresib and vehicle-treated tumors after 4 weeks of treatment. n ranges from 2-5 for different PDX. Mean ± SEM. 2-tailed unpaired t-test. HNF score of PDXs is shown on top of the graph.

(**B**) Representative images of HNF4G and HNF1A IHC in LuCaP PDX tissue microarrays at a lower (6X) and higher magnification (40X) (n=3).

(**C**) Correlation between 11-gene HNF sum Z score and HNF4G and HNF1A immunohistochemical stain-based H-scores of each PDX shown in figure 5B. Pearson's correlation coefficient and P are indicated on each plot.

(**D**) Representative images of HNF4G and HNF1A IHC in selected LuCaP PDXs when treated with pelabresib or vehicle control. Scale bar is 100 μm.

(E) Scatter plots of HNF1A IHC H-scores in vehicle and pelabresib treated PDX tumors. Mean ± SEM. 2-tailed unpaired t-test.

(**F**) Scatter plots of HNF1A IHC H-scores in vehicle and pelabresib treated PDX tumors. Mean ± SEM. 2-tailed unpaired t-test.

Figure 6. Pelabresib treatment inhibits proliferation, and induces senescence in LuCaP 70CR

(**A**) UMAPs of single cells isolated from vehicle or pelabresib-treated LuCaP 70CR tumors.

(**B**) UMAPs depicting proliferation scores of single cells isolated from vehicle or pelabresib-treated tumors.

(**C**) UMAPs depicting senescence scores of single cells isolated from vehicle or pelabresib-treated tumors.

(**D**) Representative immunohistochemical staining and quantification of Ki67 and p21 in pelabresib or vehicle-treated tumors and quantification. See methods for details. Scale bar, 100 μm. n=2. 2-tailed unpaired t-test.

(**E**) Violin plot of HNF1A expression in single cells obtained from pelabresib or vehicle treated tumors. The median is shown by a solid line while the first and third quartiles are shown by dashed lines. P value is obtained from unpaired t-test.

(**F**) Violin plot of HNF4G expression in single cells obtained from vehicle or pelabresib-treated tumors. The median is shown by a solid line while the first and third quartiles are shown by dashed lines. P value is obtained from unpaired t-test.

(**G**) Representative immunohistochemical staining and quantification of HNF1A and HNF4G in pelabresib or vehicle treated tumors and quantification (n=2). See methods for details. Scale bar, 100 μm. n=2. 2-tailed unpaired t-test.

(**H**) Violin plot depicting HNF score in single cells obtained from vehicle or pelabresib-treated tumors. The median is shown by a solid line while the first and third quartiles are shown by dashed lines. P value is obtained from unpaired t-test.

(**I**) Violin plot depicting AR expression in single cells obtained from vehicle or pelabresib-treated tumors. The median is shown by a solid line while the first and third quartiles are shown by dashed lines. P value is obtained from unpaired t-test.

(**J**) Violin plot depicting AR score in single cells obtained from vehicle or pelabresib-treated tumors. The median is shown by a solid line while the first and third quartiles are shown by dashed lines. P value is obtained from unpaired t-test.

Figure 7. Combination efficacy of enzalutamide and pelabresib in AR-positive CRPC PDX models.

(**A**) Treatment response of LuCaP 70CR PDX in SCID mice when treated with vehicle (0.5% methylcellulose/0.2% tween-80 in sterile water), enzalutamide (50 mg/kg), pelabresib (30 mg/kg), or enzalutamide and pelabresib. Enzalutamide and pelabresib were oral gavaged once and twice a day respectively (n=5 for all treatments). Treatment was started when tumors reached a volume of approximately 100 mm^3. Fold change in growth rate over day 0 (start of treatment) is shown. Mean ± SEM. 2-tailed unpaired t-test.

(**B**) Immunoblots of three representative tumor explants obtained at the end of the experiment shown in A.

(**C**) qRT-PCR analysis of HNF1A, MUC13, TMPRSS2, and KLK3 mRNA levels in tumors harvested at the end of the study. n=3 for each treatment condition.

(**D**) Treatment response of LuCaP 35CR PDX in SCID mice when treated with vehicle, enzalutamide, pelabresib, or enzalutamide and pelabresib. Treatment conditions were same as

described in A (n=3 for all treatments). Fold change in growth rate over day 0 (start of treatment) is shown. Mean ± SEM. 2-tailed unpaired t-test.

(**E**) Immunoblots of two representative tumors obtained at the end of the study shown in D.

(**F**) Left panel shows HNF score modulation in LuCaP 35CR tumors treated with different drugs as shown in D. The HNF score was calculated using RNA-Seq gene expression generated from explanted tumors at the end of the study. The right panel shows modulation of AR signaling using the AR score. 2-tailed unpaired t-test, n=3.

(**G**) Treatment response of LuCaP 77CR PDX in SCID mice when treated with vehicle, enzalutamide, pelabresib, or enzalutamide and pelabresib. Treatment conditions were same as described in A (n=3 for all treatments). Fold change in growth rate over day 0 (start of treatment) is shown. Mean ± SEM. 2-tailed unpaired t-test.

(**H**) Immunoblots of three representative tumors obtained at the end of the study shown in G.

(**I**) HNF score (left) and AR score (right) modulation in LuCaP 77CR tumors treated with different drugs as shown in G.

(**J**) Treatment response of LuCaP 49, LuCaP 145.2, and LuCaP 93 PDXs in SCID mice when treated with vehicle, enzalutamide, pelabresib or enzalutamide and pelabresib. Treatment conditions were same as described in A. n=3 for each treatment condition in each PDX line. 2-tailed unpaired t-test, n=2

Figure 1

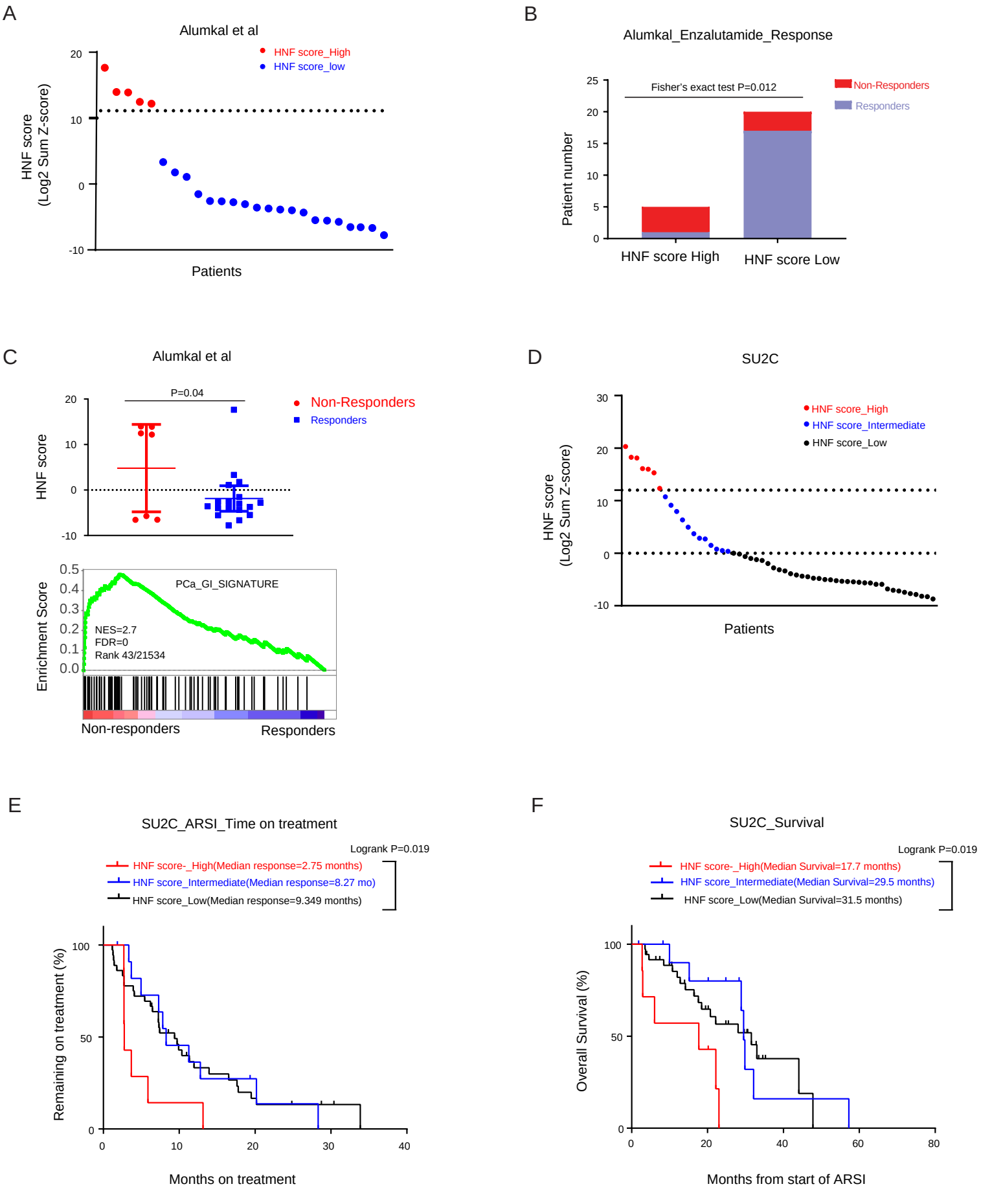
A
Alumkal et al
HNF score_High
HNF score_low
HNF score (Log2 Sum Z-score)
Patients
B
Alumkal_Enzalutamide_Response
Fisher's exact test P=0.012
Non-Responders
Responders
Patient number
HNF score High
HNF score Low
C
Alumkal et al
P=0.04
Non-Responders
Responders
HNF score
PCa_GI_SIGNATURE
NES=2.7
FDR=0
Rank 43/21534
Enrichment Score
Non-responders
Responders
D
SU2C
HNF score_High
HNF score_Intermediate
HNF score_Low
HNF score (Log2 Sum Z-score)
Patients
E
SU2C_ARSI_Time on treatment
Logrank P=0.019
HNF score-_High(Median response=2.75 months)
HNF score_Intermediate(Median response=8.27 mo)
HNF score_Low(Median response=9.349 months)
Remaining on treatment (%)
Months on treatment
F
SU2C_Survival
Logrank P=0.019
HNF score-_High(Median Survival=17.7 months)
HNF score_Intermediate(Median Survival=29.5 months)
HNF score_Low(Median Survival=31.5 months)
Overall Survival (%)
Months from start of ARSI

Figure 1. A high HNF score in CRPC correlates with adverse clinical outcomes.

(**A**) Patient stratification based on HNF scores in the Alumkal dataset. Each dot represents one patient. HNF score was calculated as the log2 sum z-score of mRNA expression of eleven genes. A sum z-score of >=12 was annotated as a high HNF score and <12 as a low HNF score. See methods for details.

(**B**) Enzalutamide response of patient tumors with high and low HNF scores. Statistical significance is determined using Fisher's exact test.

(**C**) Comparison of HNF scores between enzalutamide non-responders and responders (top) and GSEA plot of PCa_GI Gene signature (bottom) in enzalutamide non-responders compared to responders. *P* by unpaired, 2-tailed t-test. NES: Normalized enrichment score. FDR: False discovery rate.

(**D**) Patient stratification based on HNF score expression in SU2C dataset. Each dot represents one patient. Tumors with a sum z-score of >=12 were annotated as expressing high HNF score; <=0 as low HNF score and a value between 0-12 as intermediate HNF_score. See methods for details.

(**E**) Kaplan–Meier curve comparing ARSI outcome measures between the three groups stratified by HNF scores. *P* by log-rank (Mantel-Cox) test.

(**F**) Kaplan–Meier curve comparing overall survival outcome between the three groups stratified by HNF scores. *P* by log-rank (Mantel-Cox) test.

Figure 2

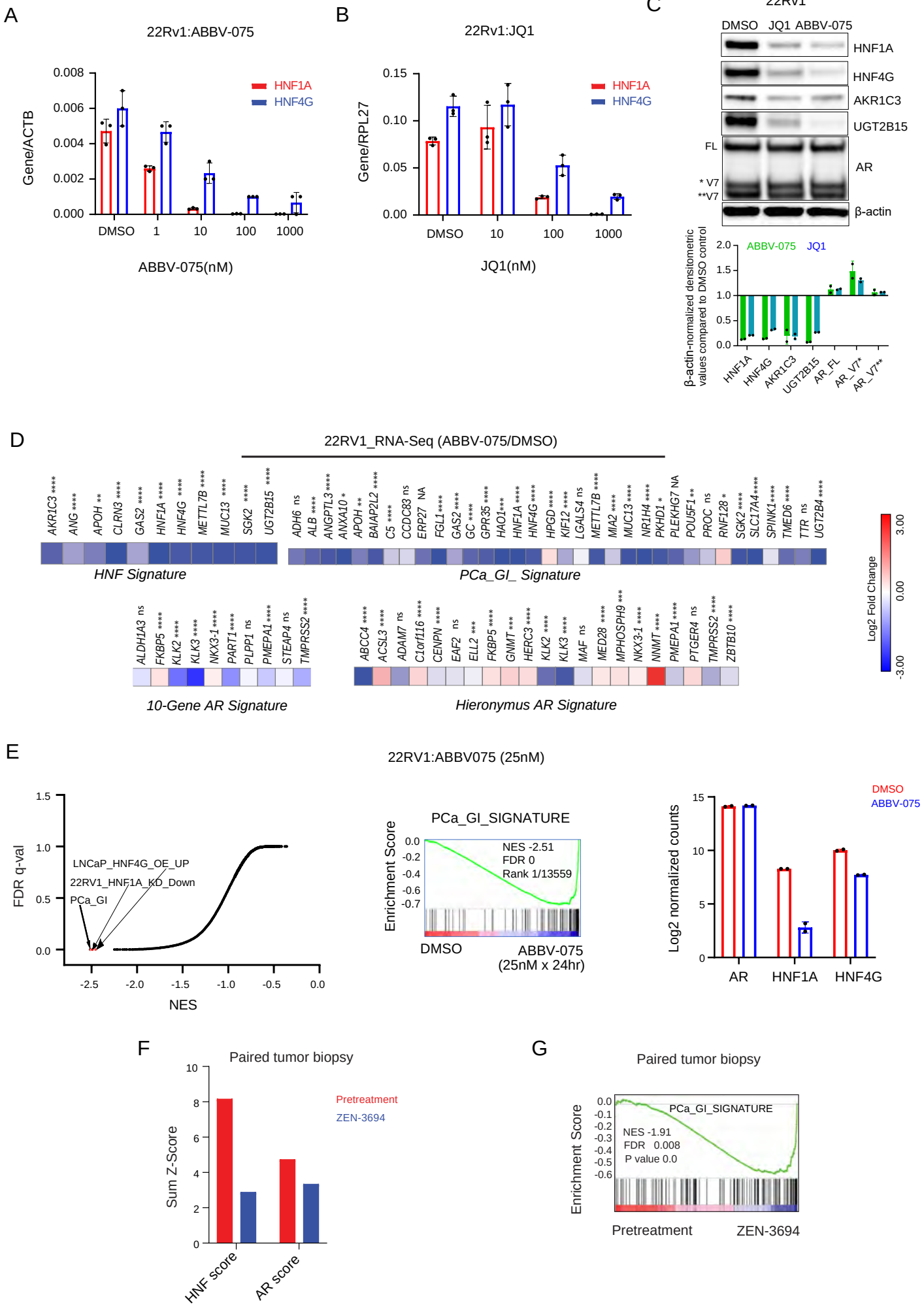
A
22Rv1:ABBV-075
Gene/ACTB
HNF1A
HNF4G
ABBV-075(nM)
B
22Rv1:JQ1
Gene/RPL27
JQ1(nM)
C
22Rv1
DMSO JQ1 ABBV-075
HNF1A
HNF4G
AKR1C3
UGT2B15
FL
AR
* V7
**V7
β-actin
β-actin-normalized densitometric values compared to DMSO control
ABBV-075 JQ1
D
22RV1_RNA-Seq (ABBV-075/DMSO)
HNF Signature
PCa_GI_ Signature
10-Gene AR Signature
Hieronymus AR Signature
Log2 Fold Change
E
22RV1:ABBV075 (25nM)
FDR q-val
LNCaP_HNF4G_OE_UP
22RV1_HNF1A_KD_Down
PCa_GI
NES
PCa_GI_SIGNATURE
Enrichment Score
NES -2.51
FDR 0
Rank 1/13559
DMSO
ABBV-075
(25nM x 24hr)
Log2 normalized counts
DMSO
ABBV-075
AR
HNF1A
HNF4G
F
Paired tumor biopsy
Sum Z-Score
Pretreatment
ZEN-3694
HNF score
AR score
G
Paired tumor biopsy
PCa_GI_SIGNATURE
Enrichment Score
NES -1.91
FDR 0.008
P value 0.0
Pretreatment
ZEN-3694

Figure 2. BET inhibitors downregulate the expression of *HNF4G* and *HNF1A* and their transcriptional signature.

(**A**) qRT-PCR showing expression of HNF1A after 4 hours of treatment with ABBV-075 and JQ1 at indicated doses.

(**B**) qRT-PCR showing expression of HNF4G after 4 hours of treatment with ABBV-075 and JQ1 at indicated doses.

(**C**) A representative immunoblot of 22Rv1 cells treated with JQ (0.5 μM), ABBV-075 (50 nM), and DMSO control for 24 hours against the indicated proteins (top) and (bottom) bar graph showing fold change in β-actin normalized band intensities of JQ1 and ABBV-075 treated samples over DMSO controls (n=2).

(**D**) Heatmap of RNA-Seq expression of HNF signature genes in 22Rv1 cells after treatment with 25 nM ABBV-075 for 24 hours (top). The two bottom heatmaps show the modulation of AR target genes with ABBV-075 treatment using two different AR gene signatures. Data is plotted as the log2 difference in gene expression between ABBV-075 and DMSO treated cells. Unadjusted P-values are shown: *P < 0.05, **P < 0.01, ***P < 0.001, and ****P < 0.0001.

(**E**) Global representation of GSEA analysis of RNA-Seq gene expression data set of 22RV1 cells treated with 25 nM ABBV-075 for 24 hours. X-axis shows the normalized enrichment score, and y-axis is the FDR q-value. The PCa_GI and the HNF1A, and HNF4G-regulated gene sets are indicated in red. GSEA plot of PCa_GI gene signature is shown in the middle. A bar diagram on the right shows the expression of AR, HNF1A, and HNF4G. NES: Normalized enrichment score. FDR: False discovery rate.

(**F**) Modulation of HNF and AR scores by BETi ZEN-3694 in paired tumor biopsies of patient 101047.

(**G**) GSEA plots of PCa_GI Gene signature in ZEN-3694 treated tumors compared to pretreated tumor. NES: Normalized enrichment score. FDR: False discovery rate.

Figure 3

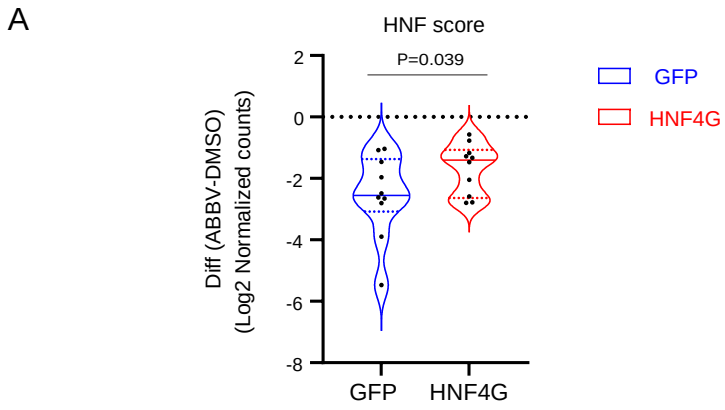
A
HNF score
P=0.039
GFP
HNF4G
Diff (ABBV-DMSO)
(Log2 Normalized counts)
2
0
-2
-4
-6
-8
GFP
HNF4G

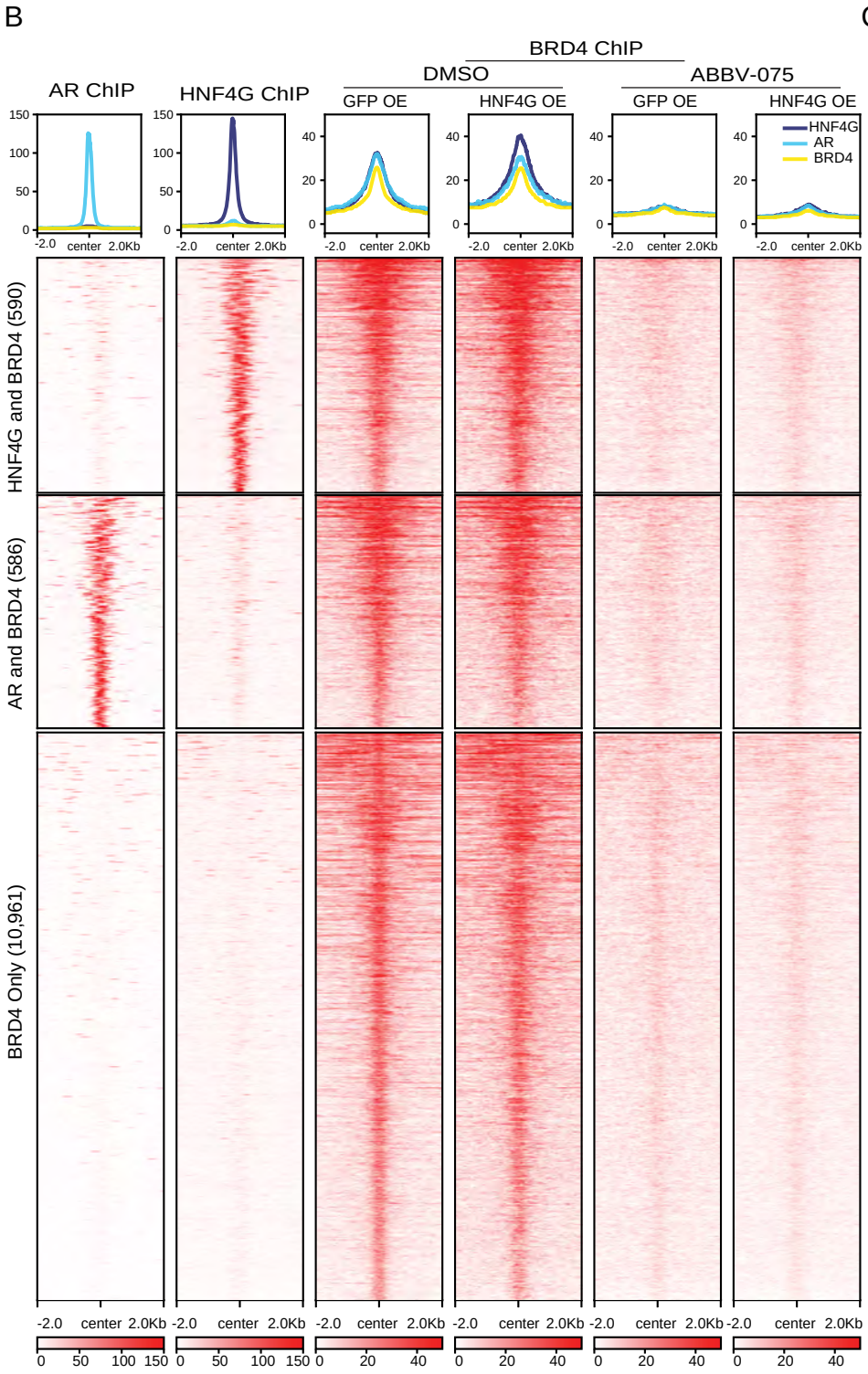
B
BRD4 ChIP
DMSO
ABBV-075
AR ChIP
HNF4G ChIP
GFP OE
HNF4G OE
GFP OE
HNF4G OE
HNF4G
AR
BRD4
HNF4G and BRD4 (590)
AR and BRD4 (586)
BRD4 Only (10,961)
-2.0 center 2.0Kb

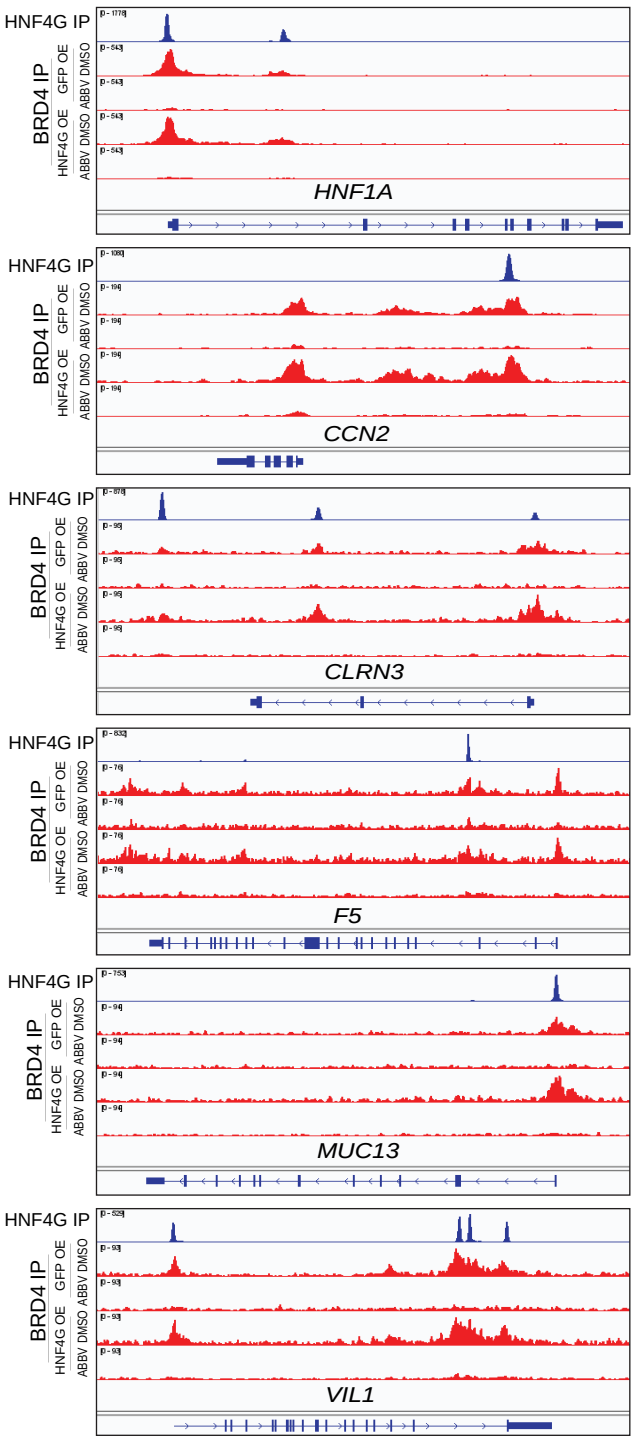
C
HNF4G IP
BRD4 IP
HNF4G OE
ABBV DMSO
GFP OE
ABBV DMSO
HNF1A
CCN2
CLRN3
F5
MUC13
VIL1

Figure 3. Inhibition of HNF4G transcription accounts for BETi mediated inhibition of GI transcriptome.

(**A**) Violin plot of log2 fold changes in expression of HNF score genes by ABBV-075 treatment in 22Rv1 cells exogenously expressing GFP or HNF4G compared with DMSO control. The median is represented by a solid line, while the first and third quartiles are indicated by dashed lines with all dots plotted. Statistical analysis was performed using a 2-tailed paired t-test.

(**B**) Histograms (top) show the average normalized tag counts of AR and HNF4G in parental 22Rv1 cells and that of BRD4 in GFP or HNF4G expressing 22Rv1 cells treated with ABBV-075 or DMSO at top 1,000 HNF4G, 1,000 AR binding sites and BRD4 only enhancer binding sites. Heatmap shows the tag densities of HNF4G, AR, and that of BRD4 at HNF4G (top) or AR (middle) binding sites. Bottom panel show the tag densities of BRD4 at 10,961 BRD4 only sites in GFP or HNF4G expressing 22Rv1 cells treated with ABBV-075 or DMSO.

(**C**) ChIP-seq profiles of HNF4G in parental 22Rv1 cells and BRD4 (DMSO treatment), and BRD4 (ABBV-075 treatment) in GFP or HNF4G expressing 22Rv1 cells at selected HNF4G target genes loci; *HNF1A*, *CCN2*, *CLRN3*, *F5*, *MUC13*, and *VIL1* in top to bottom order.

Figure 4

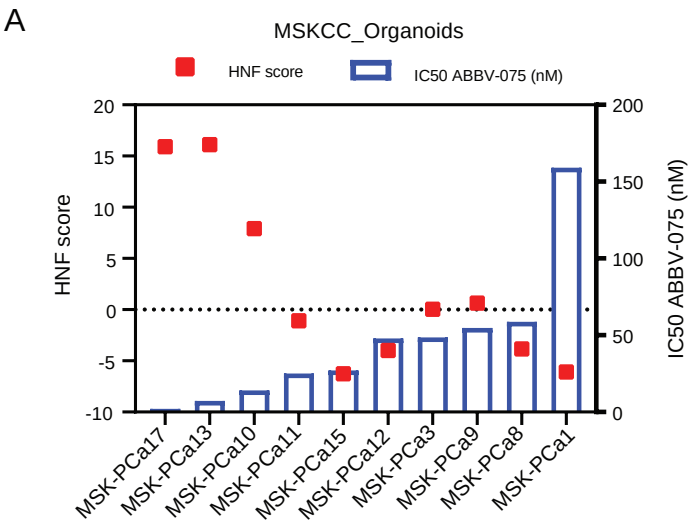
A
MSKCC_Organoids
HNF score
IC50 ABBV-075 (nM)
HNF score
IC50 ABBV-075 (nM)
MSK-PCa17
MSK-PCa13
MSK-PCa10
MSK-PCa11
MSK-PCa15
MSK-PCa12
MSK-PCa3
MSK-PCa9
MSK-PCa8
MSK-PCa1

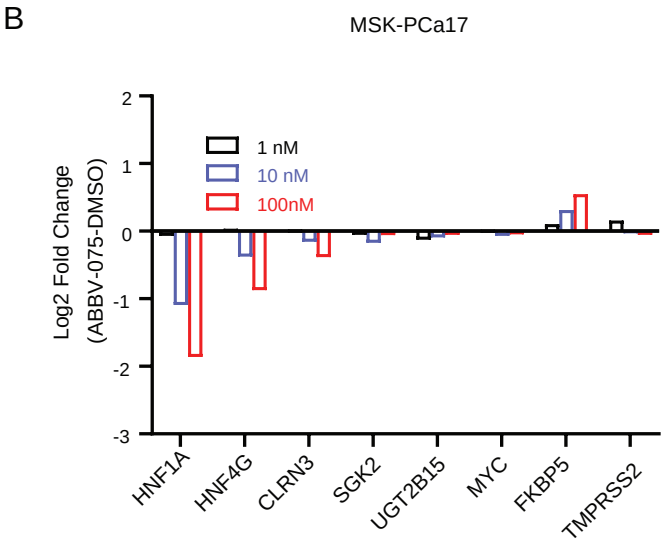
B
MSK-PCa17
1 nM
10 nM
100nM
Log2 Fold Change (ABBV-075-DMSO)
HNF1A
HNF4G
CLRN3
SGK2
UGT2B15
MYC
FKBP5
TMPRSS2

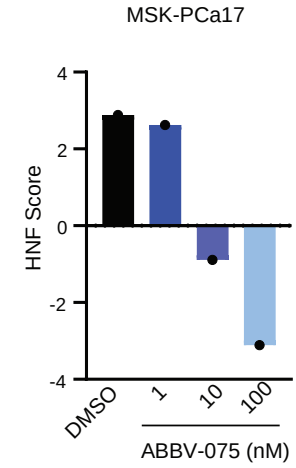
C
MSK-PCa17
HNF Score
DMSO
1
10
100
ABBV-075 (nM)

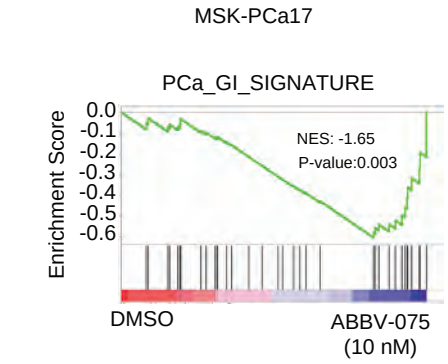
D
MSK-PCa17
PCa_GI_SIGNATURE
Enrichment Score
NES: -1.65
P-value:0.003
DMSO
ABBV-075
(10 nM)

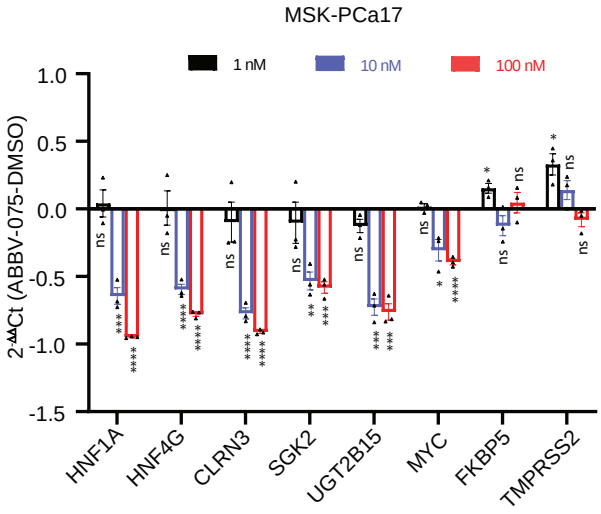
E
MSK-PCa17
1 nM
10 nM
100 nM
2-ΔΔCt (ABBV-075-DMSO)
HNF1A
HNF4G
CLRN3
SGK2
UGT2B15
MYC
FKBP5
TMPRSS2

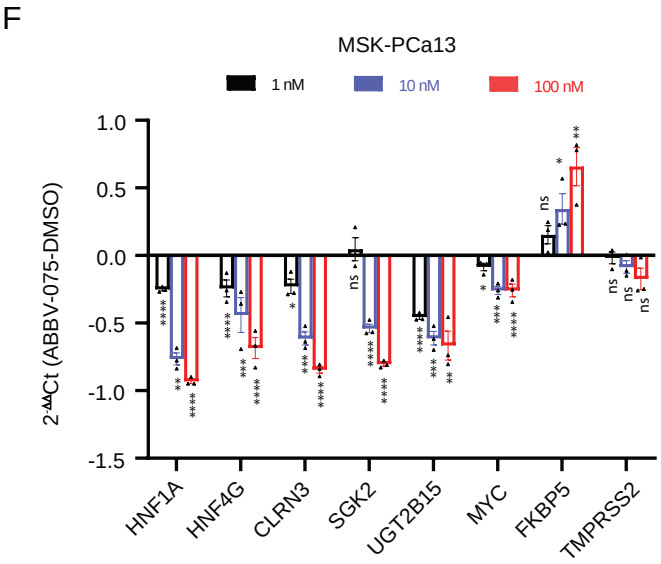
F
MSK-PCa13
1 nM
10 nM
100 nM
2-ΔΔCt (ABBV-075-DMSO)
HNF1A
HNF4G
CLRN3
SGK2
UGT2B15
MYC
FKBP5
TMPRSS2

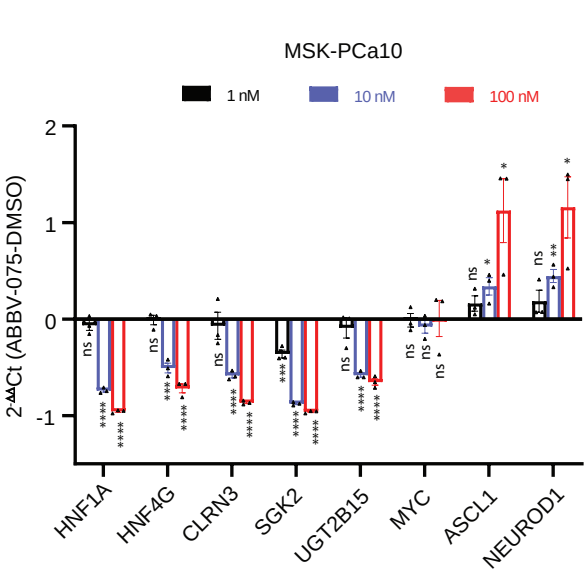
G
MSK-PCa10
1 nM
10 nM
100 nM
2-ΔΔCt (ABBV-075-DMSO)
HNF1A
HNF4G
CLRN3
SGK2
UGT2B15
MYC
ASCL1
NEUROD1

Figure 4. Patient-derived organoids with high HNF scores show increased sensitivity to BETi-mediated growth inhibition.

(**A**) IC50 of ABBV-075 in a panel of patient-derived tumor biopsies grown as organoids. The left Y-axis plots the HNF scores of each organoid and the right Y-axis shows the IC50 values.

(**B**) RNA-Seq gene expression changes of selected genes at different doses of ABBV-075 treatment of MSK-PCa17 cells compared to DMSO control. Data is presented as log2 fold difference in expression (ABBV-075 vs DMSO).

(**C**) A bar graph showing changes in HNF score expression in MSK-PCa17 cells at different doses of ABBV-075 treatment compared to DMSO control.

(**D**) GSEA analysis indicating the negative enrichment of PCa_GI gene signature gene set in MSK-PCa17 cells treated with ABBV-075 (10 nM) compared to DMSO control. NES: Normalized enrichment score.

(**E**) qRT-PCR showing expression of selected genes after 4 hours of treatment with ABBV-075 at indicated doses in MSK-PCa17 cells (n=3).

(**F**) qRT-PCR showing expression of selected genes after 4 hours of treatment with ABBV-075 at indicated doses in MSK-PCa13 cells (n=3).

(**G**) qRT-PCR showing expression of selected genes after 4 hours of treatment with ABBV-075 at indicated doses in MSK-PCa10 cells (n=3).

Unpaired, 2-tailed t-test. *P < 0.05, **P < 0.01, ***P < 0.001, and ****P < 0.0001.

Figure 5

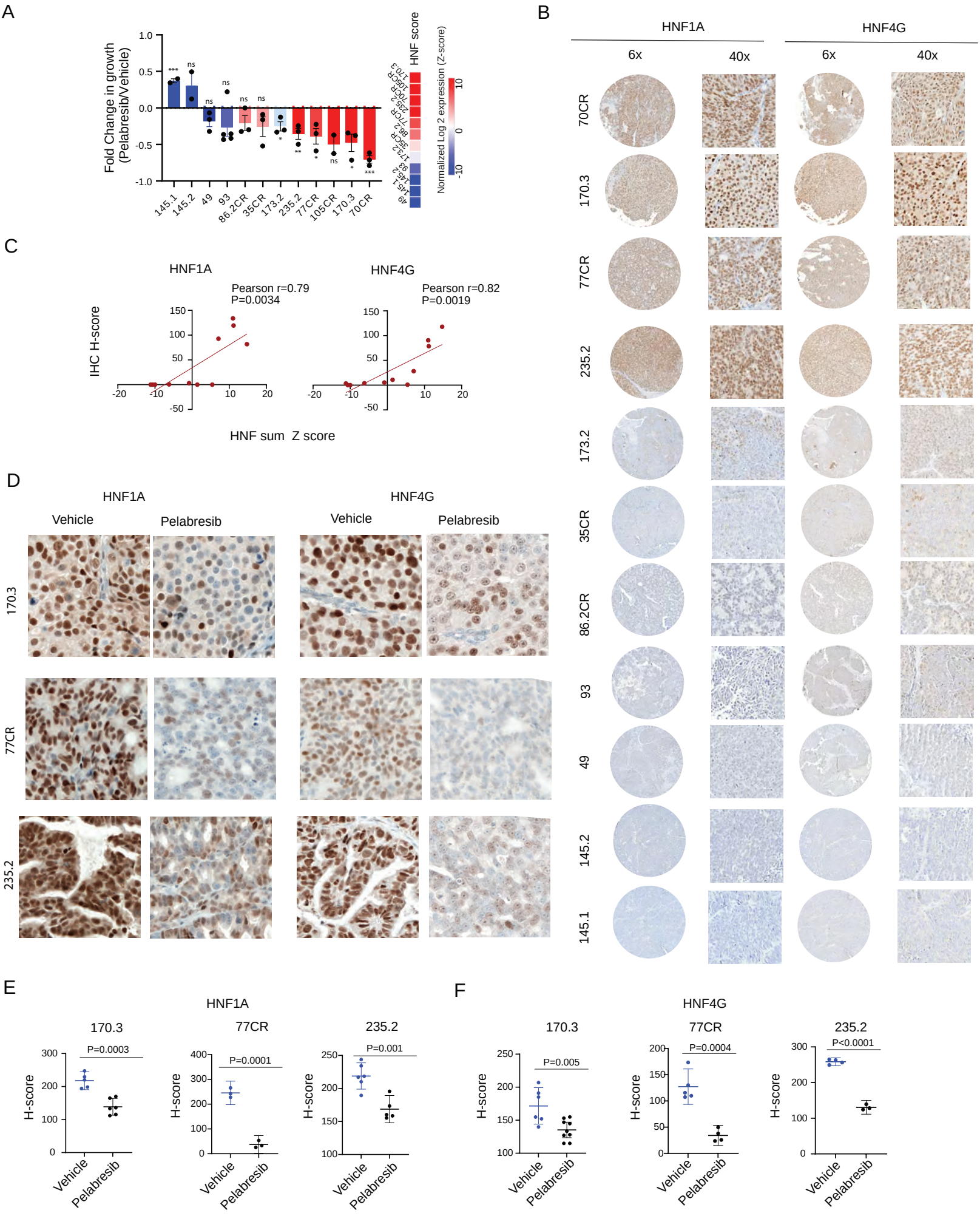
A
Fold Change in growth (Pelabresib/Vehicle)
HNF score
Normalized Log 2 expression (Z-score)
145.1
145.2
49
93
86.2CR
35CR
173.2
235.2
77CR
105CR
170.3
70CR
B
HNF1A
HNF4G
6x
40x
C
HNF1A
HNF4G
Pearson r=0.79
P=0.0034
Pearson r=0.82
P=0.0019
IHC H-score
HNF sum Z score
D
HNF1A
HNF4G
Vehicle
Pelabresib
170.3
77CR
235.2
E
HNF1A
170.3
77CR
235.2
P=0.0003
P=0.0001
P=0.001
H-score
Vehicle
Pelabresib
F
HNF4G
170.3
77CR
235.2
P=0.005
P=0.0004
P<0.0001

Figure 5. CRPC PDXs expressing high HNF score are sensitive to BET inhibition.

(**A**) Treatment response of LuCaP PDXs when treated with pelabresib (30 mg/kg) or vehicle (1% carboxymethyl cellulose) twice a day. Treatment was started when tumors reached a volume of approximately 100 mm^3. Data is plotted as the fold change in tumor volume between pelabresib and vehicle-treated tumors after 4 weeks of treatment. n ranges from 2-5 for different PDX. Mean ± SEM. 2-tailed unpaired t-test. HNF score of PDXs is shown on top of the graph.

(**B**) Representative images of HNF4G and HNF1A IHC in LuCaP PDX tissue microarrays at a lower (6X) and higher magnification (40X) (n=3).

(**C**) Correlation between 11-gene HNF sum Z score and HNF4G and HNF1A immunohistochemical stain-based H-scores of each PDX shown in figure 5B. Pearson's correlation coefficient and P are indicated on each plot.

(**D**) Representative images of HNF4G and HNF1A IHC in selected LuCaP PDXs when treated with pelabresib or vehicle control. Scale bar is 100 µm.

(E) Scatter plots of HNF1A IHC H-scores in vehicle and pelabresib treated PDX tumors. Mean ± SEM. 2-tailed unpaired t-test.

(**F**) Scatter plots of HNF1A IHC H-scores in vehicle and pelabresib treated PDX tumors. Mean ± SEM. 2-tailed unpaired t-test.

Figure 6

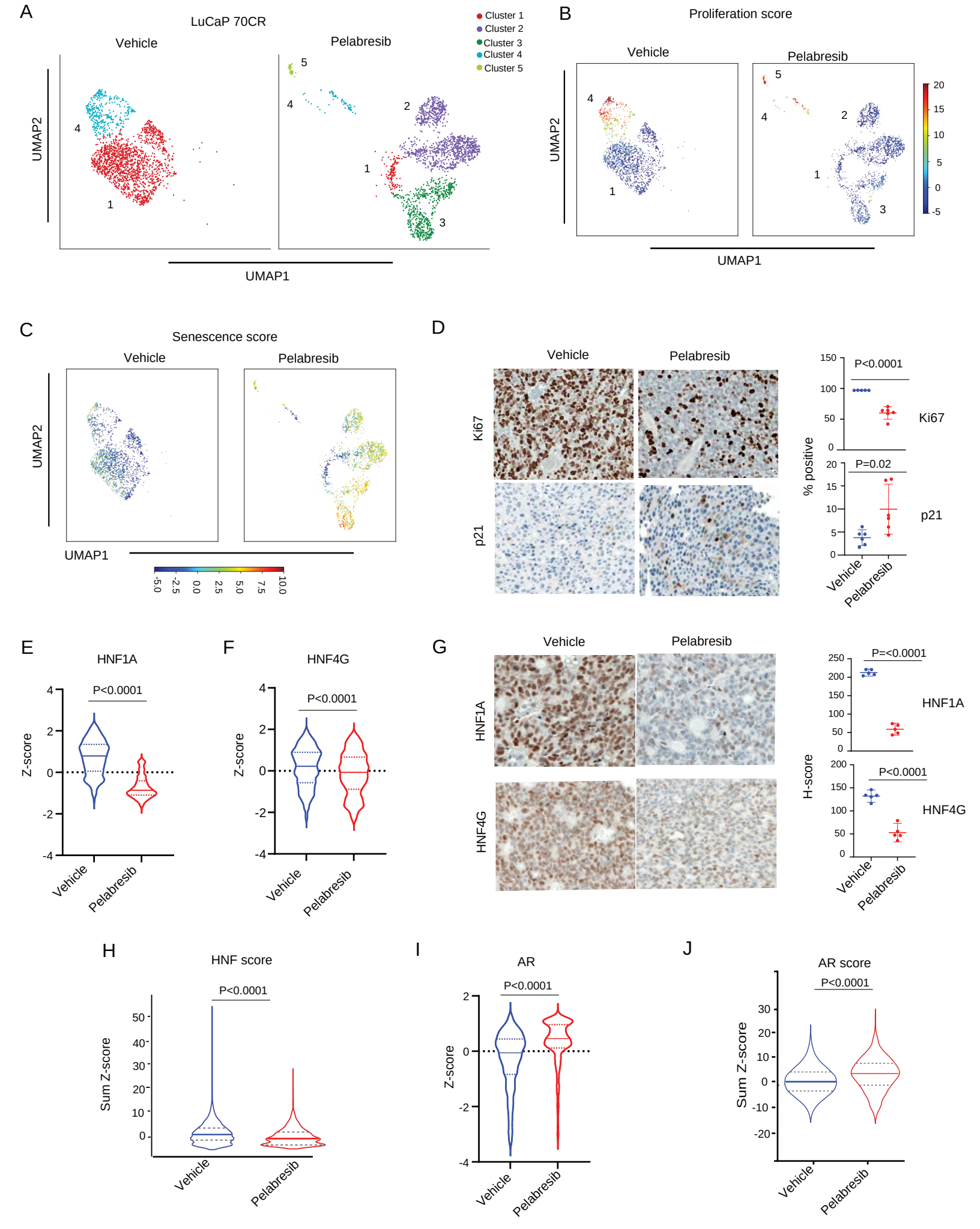
A
LuCaP 70CR
Vehicle
Pelabresib
Cluster 1
Cluster 2
Cluster 3
Cluster 4
Cluster 5
UMAP2
UMAP1
B
Proliferation score
Vehicle
Pelabresib
C
Senescence score
D
Ki67
p21
P<0.0001
P=0.02
% positive
E
HNF1A
F
HNF4G
G
H-score
H
HNF score
Sum Z-score
I
AR
Z-score
J
AR score

Figure 6. Pelabresib treatment inhibits proliferation, and induces senescence in LuCaP 70CR

(**A**) UMAPs of single cells isolated from vehicle or pelabresib-treated LuCaP 70CR tumors.

(**B**) UMAPs depicting proliferation scores of single cells isolated from vehicle or pelabresib-treated tumors.

(**C**) UMAPs depicting senescence scores of single cells isolated from vehicle or pelabresib-treated tumors.

(**D**) Representative immunohistochemical staining and quantification of Ki67 and p21 in pelabresib or vehicle-treated tumors and quantification. See methods for details. Scale bar, 100 μm. n=2. 2-tailed unpaired t-test.

(**E**) Violin plot of HNF1A expression in single cells obtained from pelabresib or vehicle treated tumors. The median is shown by a solid line while the first and third quartiles are shown by dashed lines. P value is obtained from unpaired t-test.

(**F**) Violin plot of HNF4G expression in single cells obtained from vehicle or pelabresib-treated tumors. The median is shown by a solid line while the first and third quartiles are shown by dashed lines. P value is obtained from unpaired t-test.

(**G**) Representative immunohistochemical staining and quantification of HNF1A and HNF4G in pelabresib or vehicle treated tumors and quantification (n=2). See methods for details. Scale bar, 100 μm. n=2. 2-tailed unpaired t-test.

(**H**) Violin plot depicting HNF score in single cells obtained from vehicle or pelabresib-treated tumors. The median is shown by a solid line while the first and third quartiles are shown by dashed lines. P value is obtained from unpaired t-test.

(**I**) Violin plot depicting AR expression in single cells obtained from vehicle or pelabresib-treated tumors. The median is shown by a solid line while the first and third quartiles are shown by dashed lines. P value is obtained from unpaired t-test.

(**J**) Violin plot depicting AR score in single cells obtained from vehicle or pelabresib-treated tumors. The median is shown by a solid line while the first and third quartiles are shown by dashed lines. P value is obtained from unpaired t-test.

Figure 7

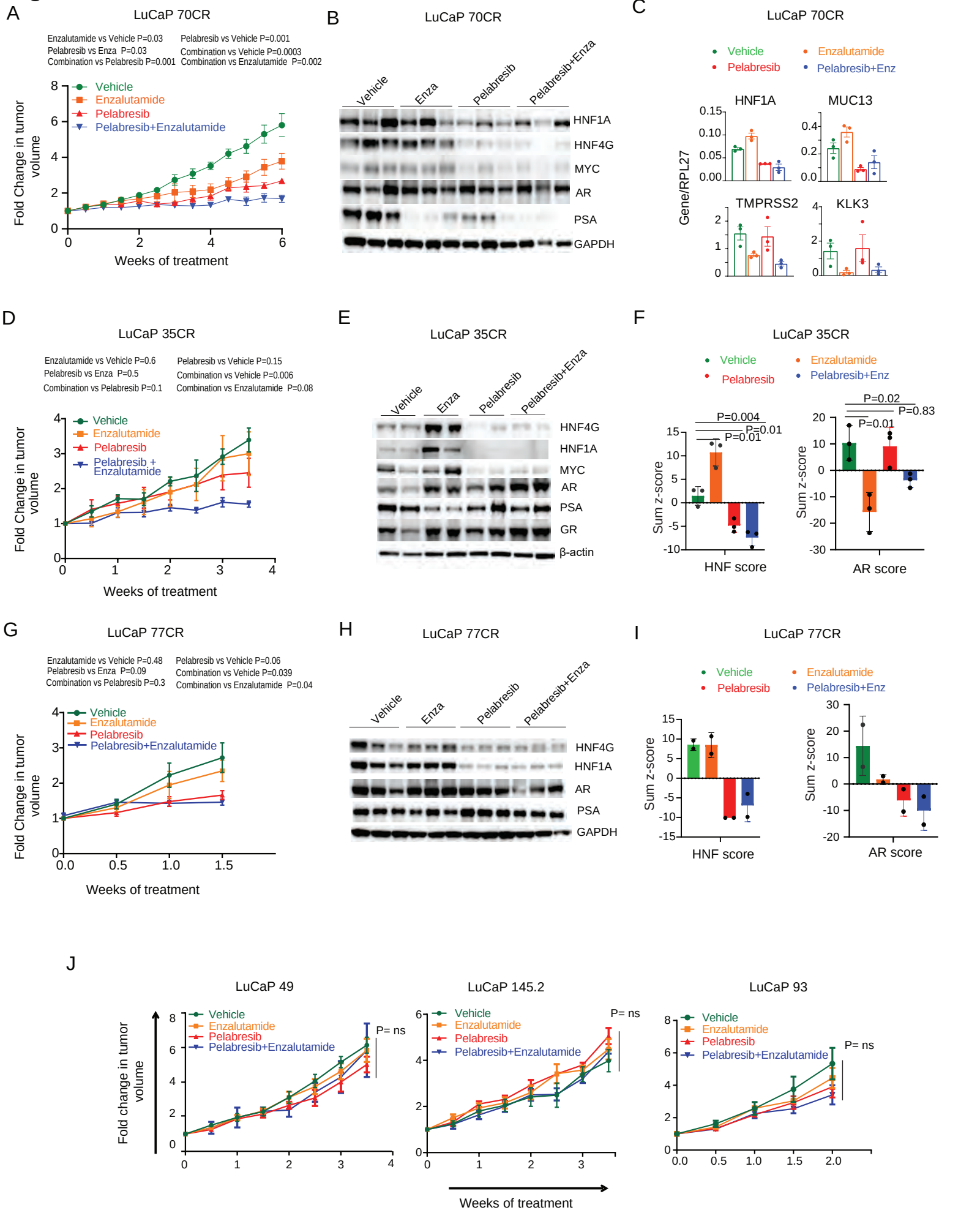
A
LuCaP 70CR
Enzalutamide vs Vehicle P=0.03
Pelabresib vs Enza P=0.03
Combination vs Pelabresib P=0.001
Pelabresib vs Vehicle P=0.001
Combination vs Vehicle P=0.0003
Combination vs Enzalutamide P=0.002
Vehicle
Enzalutamide
Pelabresib
Pelabresib+Enzalutamide
Fold Change in tumor volume
Weeks of treatment
B
LuCaP 70CR
Vehicle
Enza
Pelabresib
Pelabresib+Enza
HNF1A
HNF4G
MYC
AR
PSA
GAPDH
C
LuCaP 70CR
Vehicle
Enzalutamide
Pelabresib
Pelabresib+Enz
HNF1A
MUC13
TMPRSS2
KLK3
Gene/RPL27
D
LuCaP 35CR
Enzalutamide vs Vehicle P=0.6
Pelabresib vs Enza P=0.5
Combination vs Pelabresib P=0.1
Pelabresib vs Vehicle P=0.15
Combination vs Vehicle P=0.006
Combination vs Enzalutamide P=0.08
Vehicle
Enzalutamide
Pelabresib
Pelabresib + Enzalutamide
Fold Change in tumor volume
Weeks of treatment
E
LuCaP 35CR
Vehicle
Enza
Pelabresib
Pelabresib+Enza
HNF4G
HNF1A
MYC
AR
PSA
GR
β-actin
F
LuCaP 35CR
Vehicle
Enzalutamide
Pelabresib
Pelabresib+Enz
P=0.004
P=0.01
P=0.01
P=0.02
P=0.83
P=0.01
Sum z-score
HNF score
AR score
G
LuCaP 77CR
Enzalutamide vs Vehicle P=0.48
Pelabresib vs Enza P=0.09
Combination vs Pelabresib P=0.3
Pelabresib vs Vehicle P=0.06
Combination vs Vehicle P=0.039
Combination vs Enzalutamide P=0.04
Vehicle
Enzalutamide
Pelabresib
Pelabresib+Enzalutamide
Fold Change in tumor volume
Weeks of treatment
H
LuCaP 77CR
Vehicle
Enza
Pelabresib
Pelabresib+Enza
HNF4G
HNF1A
AR
PSA
GAPDH
I
LuCaP 77CR
Vehicle
Enzalutamide
Pelabresib
Pelabresib+Enz
Sum z-score
HNF score
AR score
J
LuCaP 49
LuCaP 145.2
LuCaP 93
Vehicle
Enzalutamide
Pelabresib
Pelabresib+Enzalutamide
P= ns
Fold change in tumor volume
Weeks of treatment

Figure 7. Combination efficacy of enzalutamide and pelabresib in AR-positive CRPC PDX models.

(**A**) Treatment response of LuCaP 70CR PDX in SCID mice when treated with vehicle (0.5% methylcellulose/0.2% tween-80 in sterile water), enzalutamide (50 mg/kg), pelabresib (30 mg/kg), or enzalutamide and pelabresib. Enzalutamide and pelabresib were oral gavaged once and twice a day respectively (n=5 for all treatments). Treatment was started when tumors reached a volume of approximately 100 mm^3. Fold change in growth rate over day 0 (start of treatment) is shown. Mean ± SEM. 2-tailed unpaired t-test.

(**B**) Immunoblots of three representative tumor explants obtained at the end of the experiment shown in A.

(**C**) qRT-PCR analysis of HNF1A, MUC13, TMPRSS2, and KLK3 mRNA levels in tumors harvested at the end of the study. n=3 for each treatment condition.

(**D**) Treatment response of LuCaP 35CR PDX in SCID mice when treated with vehicle, enzalutamide, pelabresib, or enzalutamide and pelabresib. Treatment conditions were same as described in A (n=3 for all treatments). Fold change in growth rate over day 0 (start of treatment) is shown. Mean ± SEM. 2-tailed unpaired t-test.

(**E**) Immunoblots of two representative tumors obtained at the end of the study shown in D.

(**F**) Left panel shows HNF score modulation in LuCaP 35CR tumors treated with different drugs as shown in D. The HNF score was calculated using RNA-Seq gene expression generated from explanted tumors at the end of the study. The right panel shows modulation of AR signaling using the AR score. 2-tailed unpaired t-test, n=3.

(**G**) Treatment response of LuCaP 77CR PDX in SCID mice when treated with vehicle, enzalutamide, pelabresib, or enzalutamide and pelabresib. Treatment conditions were same as

described in A (n=3 for all treatments). Fold change in growth rate over day 0 (start of treatment) is shown. Mean ± SEM. 2-tailed unpaired t-test.

(**H**) Immunoblots of three representative tumors obtained at the end of the study shown in G.

(**I**) HNF score (left) and AR score (right) modulation in LuCaP 77CR tumors treated with different drugs as shown in G.

(**J**) Treatment response of LuCaP 49, LuCaP 145.2, and LuCaP 93 PDXs in SCID mice when treated with vehicle, enzalutamide, pelabresib or enzalutamide and pelabresib. Treatment conditions were same as described in A. n=3 for each treatment condition in each PDX line. 2-tailed unpaired t-test, n=2